JOURNAL OF GEOPHYSICAL RESEARCH, VOL. 115, D12304, doi:10.1029/2009JD013250, 2010

Nighttime chemical evolution of aerosol and trace gases in a power plant plume: Implications for secondary organic nitrate and organosulfate aerosol formation, NO_3 radical chemistry, and N_2O_5 heterogeneous hydrolysis

Rahul A. Zaveri,[1] Carl M. Berkowitz,[1] Fred J. Brechtel,[2] Mary K. Gilles,[3] John M. Hubbe,[1] John T. Jayne,[4] Lawrence I. Kleinman,[5] Alexander Laskin,[6] Sasha Madronich,[7] Timothy B. Onasch,[4] Mikhail S. Pekour,[1] Stephen R. Springston,[5] Joel A. Thornton,[8] Alexei V. Tivanski,[9] and Douglas R. Worsnop[4]

Received 22 September 2009; revised 20 December 2009; accepted 15 January 2010; published 22 June 2010.

[1] Nighttime chemical evolution of aerosol and trace gases in a coal-fired power plant plume was monitored with the Department of Energy Grumman Gulfstream-1 aircraft during the 2002 New England Air Quality Study field campaign. Quasi-Lagrangian sampling in the plume at increasing downwind distances and processing times was guided by a constant-volume balloon that was released near the power plant at sunset. While no evidence of fly ash particles was found, concentrations of particulate organics, sulfate, and nitrate were higher in the plume than in the background air. The enhanced sulfate concentrations were attributed to direct emissions of gaseous H_2SO_4, some of which had formed new particles as evidenced by enhanced concentrations of nucleation-mode particles in the plume. The aerosol species were internally mixed and the particles were acidic, suggesting that particulate nitrate was in the form of organic nitrate. The enhanced particulate organic and nitrate masses in the plume were inferred as secondary organic aerosol, which was possibly formed from NO_3 radical-initiated oxidation of isoprene and other trace organic gases in the presence of acidic sulfate particles. Microspectroscopic analysis of particle samples suggested that some sulfate was in the form of organosulfates. Microspectroscopy also revealed the presence of sp^2 hybridized C = C bonds, which decreased with increasing processing time in the plume, possibly because of heterogeneous chemistry on particulate organics. Constrained plume modeling analysis of the aircraft and tetroon observations showed that heterogeneous hydrolysis of N_2O_5 was negligibly slow. These results have significant implications for several issues related to the impacts of power plant emissions on air quality and climate.

Citation: Zaveri, R. A., et al. (2010), Nighttime chemical evolution of aerosol and trace gases in a power plant plume: Implications for secondary organic nitrate and organosulfate aerosol formation, NO_3 radical chemistry, and N_2O_5 heterogeneous hydrolysis, *J. Geophys. Res.*, *115*, D12304, doi:10.1029/2009JD013250.

1. Introduction

[2] Fossil-fuel-fired power plants in the United States contributed 18% and 66% of the national nitrogen oxides (NO_x = NO + NO_2) and sulfur dioxide (SO_2) emissions, respectively, in 2008 (http://www.epa.gov/ttn/chief/trends). The fate of these two pollutants are of major concern for a number of environmental issues, including air quality [*Unger et al.*, 2006], visibility degradation [*Malm et al.*, 1994], acid deposition [*Norris et al.*, 1999], and aerosol radiative forcing [*Forster et al.*, 2007]. While power plants themselves are not a significant source of volatile organic compounds (VOCs), the regions surrounding them, such as in the eastern United States, are often rich sources of biogenic VOCs (e.g., isoprene, monoterpenes, etc.) from natural vegetation. During the daytime, the power plant

[1]Atmospheric Sciences and Global Change Division, Pacific Northwest National Laboratory, Richland, Washington, USA.
[2]Brechtel Manufacturing, Inc., Hayward, California, USA.
[3]Chemical Sciences Division, Lawrence Berkeley National Laboratory, Berkeley, California, USA.
[4]Aerodyne Research, Inc., Billerica, Massachusetts, USA.
[5]Environmental Sciences Department, Brookhaven National Laboratory, Upton, New York, USA.
[6]Environmental Molecular Sciences Laboratory, Pacific Northwest National Laboratory, Richland, Washington, USA.
[7]National Center for Atmospheric Research, Boulder, Colorado, USA.
[8]Department of Atmospheric Sciences, University of Washington, Seattle, Washington, USA.
[9]Department of Chemistry, University of Iowa, Iowa City, Iowa, USA.

0148-0227/10/2009JD013250

emissions tend to disperse throughout the turbulent boundary layer and readily mix with the freshly emitted biogenic VOCs. In the presence of sunlight and VOCs, NO_x catalyzes photochemical ozone (O_3) formation [*Gillani et al.*, 1998; *Ryerson et al.*, 2001; *Frost et al.*, 2006, and references therein]. NO_x photochemistry also influences secondary organic aerosol (SOA) formation from biogenic VOCs both directly via the SOA yield and indirectly via the effect of NO_x on oxidant abundance [*Kroll et al.*, 2005, 2006; *Ng et al.*, 2007]. Moreover, oxidation of SO_2 and NO_2 with the photochemically produced OH radicals forms sulfuric acid (H_2SO_4) and nitric acid (HNO_3), respectively, both of which can condense onto preexisting particles [*Meagher et al.*, 1978; *McMurry et al.*, 1981; *Hobbs and Hegg*, 1982; *Hegg et al.*, 1985; *Brock et al.*, 2002]. In addition, H_2SO_4 molecules can also nucleate to form new particles [*Whitby et al.*, 1978; *Wilson and McMurry*, 1981].

[3] Hot power plant emissions released at night typically rise above the stable surface layer and tend to remain highly concentrated in the vertically stratified residual layer [*Smith et al.*, 1978; *Brown et al.*, 2007]. Significant chemical processing can also occur in such nocturnal power plant plumes for several hours before they are diluted due to turbulent mixing the following morning. For instance, the emitted NO rapidly reacts with O_3 to form NO_2, which gradually reacts further with O_3 to form the nitrate radical (NO_3). Subsequent reactions of NO_3 have the potential to cause further irreversible destruction of O_3 during the course of a night. Depending on the ambient temperature, NO_3 reacts rapidly and reversibly with NO_2 to form dinitrogen pentoxide (N_2O_5), which can undergo heterogeneous hydrolysis on aerosol particles to form HNO_3 [*Brown et al.*, 2003, 2004]. NO_3 can also react with biogenic VOCs and their oxidation products that remain in the nocturnal residual layer from the preceding afternoon and possibly form SOA consisting of low-volatility organic nitrates [*Barnes et al.*, 1990; *Shepson et al.*, 1996; *Starn et al.*, 1998; *Ng et al.*, 2008; *Fry et al.*, 2009; *Rollins et al.*, 2009]. In maritime atmospheres, the NO_3 reaction with dimethyl sulfide (DMS) to form HNO_3 becomes important as well [*Stark et al.*, 2007].

[4] In the absence of appreciable levels of OH radicals, SO_2 undergoes little change at night. However, trace amounts of gaseous SO_3/H_2SO_4 (<1% of SO_2 emissions) may concomitantly be emitted from power plants [*Mueller and Imhoff*, 1994; *Srivastava et al.*, 2004; *Cichanowicz*, 2007]. Upon cooling, these gases can potentially nucleate to form new particles in the nighttime plume. Reactive uptake of biogenic VOCs and their photo-oxidation products on such acidic sulfate particles are known to form organosulfate SOA [*Liggio and Li*, 2006; *Liggio et al.*, 2007; *Paulot et al.*, 2009] or nitroxy organosulfate SOA in the presence of NO_3 radicals [*Surratt et al.*, 2008].

[5] The overall rate and efficiency with which NO_x is converted to HNO_3 and organic nitrates at night is of great interest, because at dawn the residual NO_3 and N_2O_5 can photolyze or dissociate back to NO_x and subsequently produce O_3 in the presence of VOCs [*Dentener and Crutzen*, 1993]. At the same time, SOA formation via reactions between power plant emissions and biogenic VOCs at night is of relevance to air quality, regional haze, and climate issues. Nighttime SOA formation may also affect the N_2O_5 heterogeneous hydrolysis uptake coefficient $\gamma(N_2O_5)$, which ranges between <0.001 and 0.1 depending on the particle composition, acidity, phase state, and relative humidity and water content [*Mozurkewich and Calvert*, 1988; *Hu and Abbatt*, 1997; *Wahner et al.*, 1998; *Kane et al.*, 2001; *Folkers et al.*, 2003; *Hallquist et al.*, 2003; *Thornton et al.*, 2003; *Thornton and Abbatt*, 2005; *Brown et al.*, 2006b, 2009; *Bertram and Thornton*, 2009].

[6] Very few airborne studies have focused on the nighttime transport and transformation of power plant plumes relative to similar studies carried out during the daytime. It is not only difficult to carry out nighttime aircraft missions but also very challenging to locate vertically stratified nocturnal power plant plumes at increasing downwind distances and, hence, to make measurements describing the chemical evolution in such plumes as a function of increasing processing time. As a result, relatively little is known about the chemical processing of aerosol and trace gases in nocturnal power plant plumes.

[7] We report here on the nighttime observations of aerosol and trace gases in the Salem Harbor power plant plume made from the Department of Energy (DOE) Grumman Gulfstream-1 aircraft (G-1). These observations were made during the DOE Nighttime Aerosol-Oxidant Plume Experiment (NAOPEX), which was carried out as part of the summer 2002 New England Air Quality Study (NEAQS) field campaign. A quasi-Lagrangian aircraft sampling strategy, guided by superpressure constant-volume tetroons (tetrahedral balloons), was employed to monitor the chemical evolution of NO, NO_2, SO_2, O_3, and aerosol in the power plant plume. The paper is organized as follows. Section 2 describes the field experiment and methods pertaining to the G-1 aircraft instrumentation, the tetroon system, the quasi-Lagrangian aircraft sampling strategy, and the flight plans for the 30–31 July episode. In section 3, we first identify four distinct power plant plume segments and calculate their processing times since emission. We then present an analysis of the evolution of the NO_x/NO_y ratio with processing time and conservation of the total odd oxygen atoms in the plume. Section 3 also presents an analysis of aerosol number size distribution and composition data to reveal evidence for new particle formation and SOA formation in the plume and the presence of organic nitrates, organosulfates, and sp^2 hybridized C = C double bonds in these particles. In section 4, we present results from a constrained plume modeling (CPM) analysis of the aircraft and tetroon observations to gain further insight into the chemical processing of trace gases and estimate the N_2O_5 uptake coefficient.

2. Field Experiment and Methods

[8] The DOE G-1 aircraft conducted 17 research flights between 10 July and 11 August during the 2002 NEAQS field campaign. The daytime flights were devoted to a regional survey of aerosol precursors, composition, and microphysical properties in the southern New England and the mid-Atlantic states [*Kleinman et al.*, 2007]. The nighttime flights during NAOPEX were designed to follow the evolution of aerosols and trace gases from the Boston urban area and the nearby Salem Harbor power plant. In this study, we focus on the observations made in the power plant plume on 30–31 July 2002.

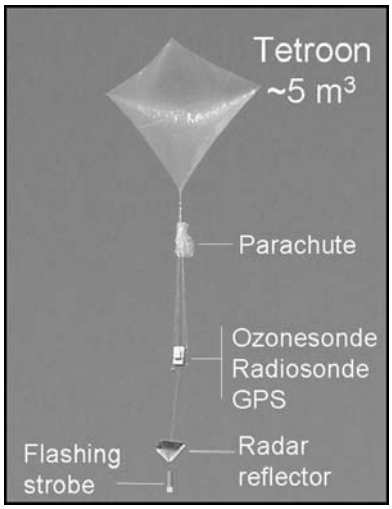

Figure 1. Superpressure tetroon system and payload assembly used in the 2002 NAOPEX field study. The total weight of the payload train was ~2.5 kg.

2.1. G-1 Aircraft Instrumentation

[9] The measurement suite on board the G-1 aircraft included O_3, SO_2, NO, NO_2, NO_y, volatile organic compounds (canister samples), aerosol size distribution, and optical properties. Aerosol chemical composition was measured with the Aerodyne Quadrupole Aerosol Mass Spectrometer (Q-AMS) [*Jayne et al.*, 2000]. Additionally, sampling of aerosol particles for microscopy and spectromicroscopic analyses was carried out using a time-resolved aerosol collector (TRAC) [*Laskin et al.*, 2003, 2006]. The standard meteorological package on the G-1 provided the ambient temperature, pressure, relative humidity, dew point, and wind-vector measurements. The details of the various instruments and detection techniques are described by *Kleinman et al.* [2007, and references therein].

2.2. Tetroon System: Lagrangian Plume Tracer

[10] A superpressure (pressure greater than the ambient atmospheric pressure) constant-volume tetroon (tetrahedral balloon) filled with an admixture of helium and air will float at an altitude at which it attains equilibrium with the surrounding air [*Angell*, 1961]. Superpressure tetroons and balloons capable of adjusting buoyancy through the action of an onboard pump and valves have been used extensively in the study of low-altitude atmospheric currents, turbulence, and vertical motions [*Hoecker*, 1975; *Angell et al.*, 1976; *Zak*, 1981] and in major Lagrangian field programs to track air pollution plumes and guide repeated aircraft sampling in the "tagged" air parcels [*Businger et al.*, 1996, 1999; *Huebert et al.*, 1996; *Johnson et al.*, 2000a, 2000b; *Fehsenfeld et al.*, 2006; *Mao et al.*, 2006; *Riddle et al.*, 2006].

[11] Superpressure tetroons (volume ~5 m^3) were used during NAOPEX as Lagrangian tracers of urban and power plant plumes under stable conditions at night. The instrument payload included a GPS transceiver and a Vaisala radiosonde to continuously measure the ambient temperature, pressure, and relative humidity in the tagged air parcel. The electrochemical concentration cell (ECC) ozonesonde [*Komhyr*, 1969; *Komhyr et al.*, 1995] with an extended operation time of up to 12 h was added to the tetroon payload to provide a Lagrangian time trace of O_3 in the tagged air parcel. The complete tetroon system assembly is shown in Figure 1. The transmitted data stream consisting of time, latitude, longitude, altitude, temperature, pressure, relative humidity, and O_3 mixing ratio was received both on the ground and on board the G-1 aircraft every 10 s via line-of-sight telemetry.

2.3. Quasi-Lagrangian Sampling Strategy

[12] A Lagrangian aircraft sampling strategy can facilitate powerful insights into the chemical processing of trace gases and aerosols by monitoring their concentrations and composition in the pollution plume as it is advected downwind from the source region [*Johnson et al.*, 2000a]. The superpressure tetroon was used as a Lagrangian tracer to "tag" the Salem Harbor power plant plume soon after sunset and guide aircraft sampling at increasing downwind distances through the night. The tetroon's GPS location received on board the G-1 aircraft was fed into a specially designed flight planning program that was used to guide the flight tracks in the vicinity of the tetroon. The resulting tetroon-based meteorological and O_3 measurements were close to being true Lagrangian (i.e., within the same air parcel). The repeated aircraft observations made within the plume at increasing downwind distances are referred to as quasi-Lagrangian because they were deliberately not made within precisely the same air parcel to avoid sampling the G-1's own exhaust from one of the previous transects. The quasi-Lagrangian measurements in the power plant plume thus describe the evolution of the emitted species from a known starting time.

[13] The Boston coastal area during July 2002 had clear nighttime skies with offshore synoptic winds in the nocturnal residual layer over the decoupled stable marine boundary layer. Under these conditions, power plant plumes emitted into the nocturnal residual layer would be in a thermodynamically stable environment, which would tend to maintain the plume identity. The overwater trajectories associated with the offshore winds minimized dry deposition losses as well as the injection of fresh emissions from below, thus reducing the complexity of data analysis.

[14] The tetroon launch site was based at Northeastern University's Marine Science Center (MSC) facility in Nahant, Massachusetts, which is an island-like coastal site ~9.5 km northeast of the Boston Logan International Airport and ~12 km south of the Salem Harbor power plant. The G-1 aircraft operation was based in Worcester, Massachusetts.

2.4. Episode During 30–31 July

[15] On the evening of 30 July 2002, the weather forecast called for clear skies and the HYSPLIT model [*Draxler and Rolph*, 2003] predicted offshore trajectories to the southeast in the nocturnal residual layer for air parcels starting over Nahant at sunset (1907 EST). It was under these favorable conditions that a tetroon was launched at 1950 EST, with the buoyancy preadjusted so that it would attain an altitude of 600–700 m above mean sea level (asl) or approximately in the center of the nocturnal residual layer, as characterized by radiosondes. This strategy does not guarantee that the bal-

loon will track the power plant plume, because the power plant plume rise is not known at the time of the balloon launch. Also, nighttime wind shear and low-level jet formation may cause difficulty in locating the plume. Nevertheless, placing the tetroon at roughly the center of the nocturnal residual layer is a reasonable strategy for increasing the likelihood of tagging the plume. Two back-to-back G-1 flights were guided by the tetroon trajectory to find and intercept the Salem Harbor power plant plume at increasing downwind distances. The first G-1 flight took place between 2040 and 2320 EST on 30 July. The second G-1 flight began at 0055 EST on 31 July and lasted until 0255 EST. The time difference between UTC and EST is 5 h (i.e., EST = UTC – 5 h).

[16] The tetroon trajectory and the G-1 aircraft flight tracks are illustrated in Figure 2. Figure 2 (top) shows the tetroon trajectory and the two G-1 flight paths while Figure 2 (bottom) displays the corresponding information in a plot of altitude versus time. The numbered yellow squares along the G-1 flight paths indicate the locations where VOC canister samples were acquired. The numbered pink hexagons indicate the locations of the TRAC particle samples selected for microscopy and microspectroscopy studies. Other features shown in these plots are described later in the text. Figure 3 illustrates the time evolution of the vertical profiles of potential temperature, wind speed, and wind direction in the nocturnal residual layer as measured by the G-1 and the tetroon during its ascent and descent. The potential temperature profiles indicate the presence of a stable surface layer below 200 m asl. The residual layer was neutrally buoyant up to 2240 EST and became relatively stable by the end of the mission at 0200 EST (31 July). Similarly, the wind speeds were fairly uniform as a function of altitude until 2240 EST, whereas a low-level nocturnal jet had developed by 0200 EST. The wind direction gradually changed from northwesterly to northeasterly through the course of the evening, but its vertical profiles remained fairly uniform at any given time. This change in wind direction is consistent with the curvature in the tetroon trajectory seen in Figure 2.

3. Data Analysis

[17] We first review the tetroon and G-1 aircraft observations in this section to characterize the chemical and physical properties of the power plant plume, and we also set up key input parameters for the model analysis that follows in section 4.

3.1. Tetroon Observations

[18] Tetroon-borne ozonesonde and radiosonde measurements of O_3, temperature, pressure, and relative humidity along the tetroon trajectory as a function of time are shown in Figure 4. The mean tetroon altitude was ~670 m asl with oscillations of ±50 m that gradually decreased during the first 3 h. The temperature at this altitude decreased from 297 to 295 K over a period of 6 h, possibly because of radiative cooling of air under clear skies at night, with a corresponding increase in relative humidity from 46% to 54%.

[19] On the basis of the evolution of these meteorological variables, it appears that the tetroon was advected in the same air parcel for 6 h. Therefore, continuous measurement of O_3 in this air parcel represents a near-ideal Lagrangian trace. Interestingly, O_3 gradually decayed from 48 to 44 ppbv during the first 3 h (1950–2250 EST), followed by a sudden drop to about 25 ppbv at 2300 EST, and remained relatively constant thereafter. The initial gradual loss in O_3, which is discussed in detail in section 4, could be attributed to the $O_3 + NO_2$ reaction. The sudden drop of ~20 ppbv at 2300 EST could be due to a malfunction in the ozone sensor or due to the tetroon drifting into a markedly different plume layer. The latter seems less likely because the altitude fluctuations were minimal and no sudden changes were observed in relative humidity (RH) when the O_3 mixing ratio rapidly decreased.

3.2. Quasi-Lagrangian Power Plant Plume Segments and Processing Times

[20] On the evening of 30 July 2002, three out of four units were operational at the Salem Harbor power plant facility. One unit utilized only residual oil while both coal (primary) and residual oil (secondary) were used to fire the other two units. Selective noncatalytic reduction low-NO_x burner technology was used to control the NO_x emissions, and electrostatic precipitators were used to control the particulate matter emissions while no emission control was used for SO_2 (Clean Air Markets, Data and Maps, EPA, http://camddataandmaps.epa.gov/gdm).

[21] Repeated aircraft vertical profiles and horizontal transects near the tetroon revealed the presence of the Salem Harbor power plant emissions at multiple altitudes in the nocturnal residual layer. The colored triangles shown in Figure 2 along the tetroon trajectory indicate the mean tetroon positions that correspond in time to the four colored segments on the G-1 flight paths. These four segments mark the locations of the Salem power plant plume as identified by the measured excesses of SO_2 and NO_y mixing ratios over the nearby background values at low and high altitudes of ~325 and ~970 m asl, respectively. The fact that these four plume segments were indeed of Salem power plant origin can be ascertained from the slopes of SO_2 versus NO_y correlations (Figure 5), which are similar to each other and in very good agreement with the overall SO_2/NO_x emission ratio of ~2 mol/mol for this power plant, reported specifically for the evening of 30 July 2002 (Clean Air Markets, Data and Maps, EPA, http://camddataandmaps.epa.gov/gdm). The water vapor mixing ratio was uniformly distributed in each plume segment and the RH was fairly steady between 60% and 70%.

[22] Because all four plume segments were in the nocturnal residual layer that was effectively decoupled from the stable marine boundary layer, we assume that they experienced negligible dry deposition losses. The light blue (low-altitude, "A-low") and dark blue (high-altitude, "A-high") segments were measured during the first G-1 flight and represent relatively less aged emissions. The orange (low-altitude, "B-low") and red (high-altitude, "B-high") segments were measured farther downwind during the second G-1 flight and are therefore relatively more aged. These four plume segments were restricted to two distinct altitudes, with the mean tetroon altitude located roughly in the center. This provided consistency in comparing the fresh and aged plume segments at the same altitudes.

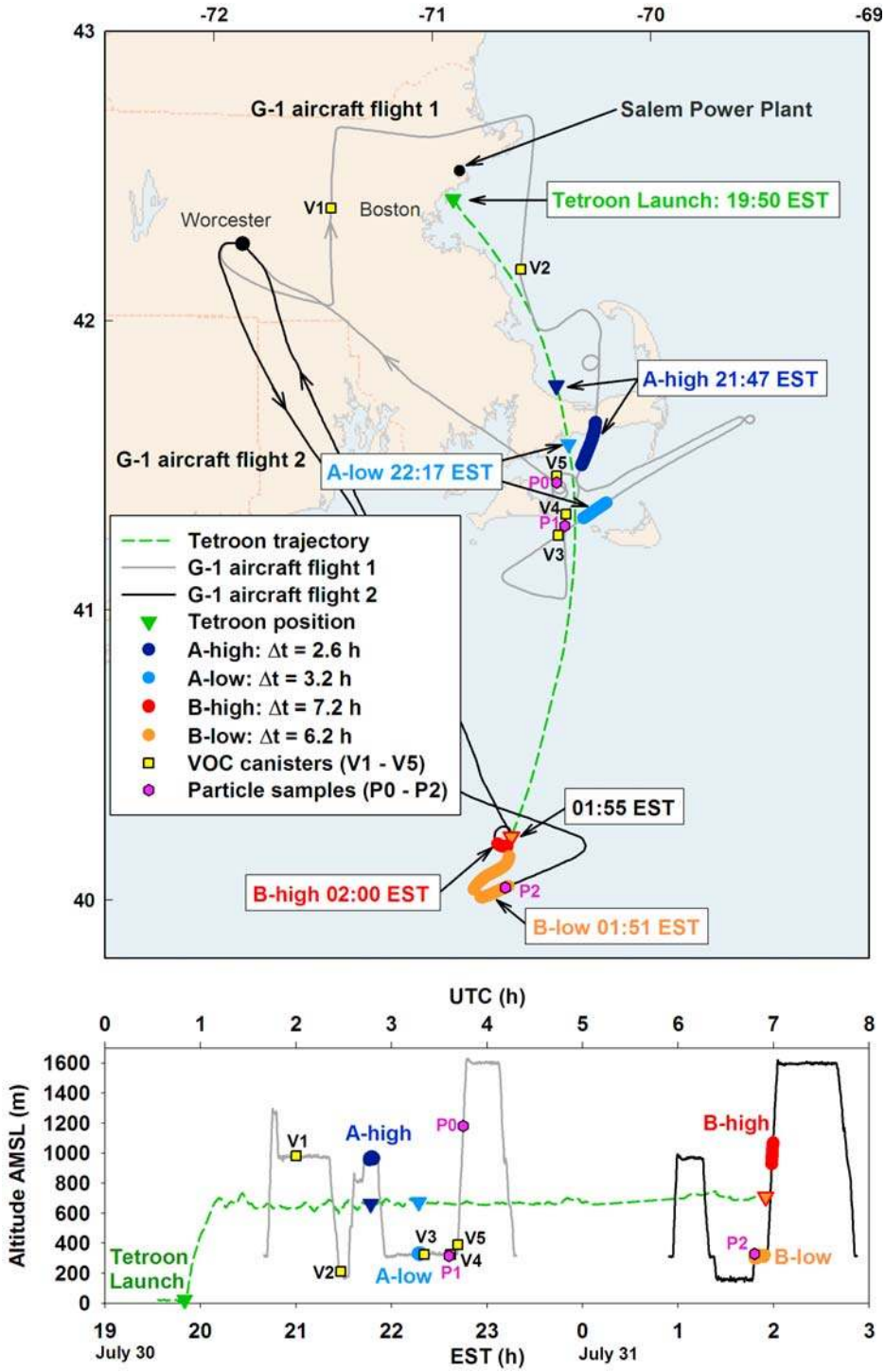

Figure 2. (Top) The tetroon trajectory (dotted green line) and the two G-1 aircraft flight paths (gray and black lines) for the 30–31 July episode. (Bottom) G-1 aircraft and tetroon flight altitudes plotted as a function of time. Colored triangles indicate the positions of the tetroon when the G-1 intercepted segments of the Salem Harbor power plant plume (marked with circles of corresponding colors) at increasing processing times (Δt) since emission. Yellow squares and pink hexagons indicate the locations where VOC canisters and TRAC particle samples, respectively, were collected and analyzed.

[23] In combination, Figures 2 and 3 provide a three-dimensional picture as a function of time and space of the power plant plume segments (as sampled by the G-1 aircraft) relative to the tetroon positions and the evolution of the residual boundary layer. The relative spatial proximities between the tetroon and the power plant plume segments and the observed vertical wind velocity profiles near the tetroon were used to estimate the postemission processing

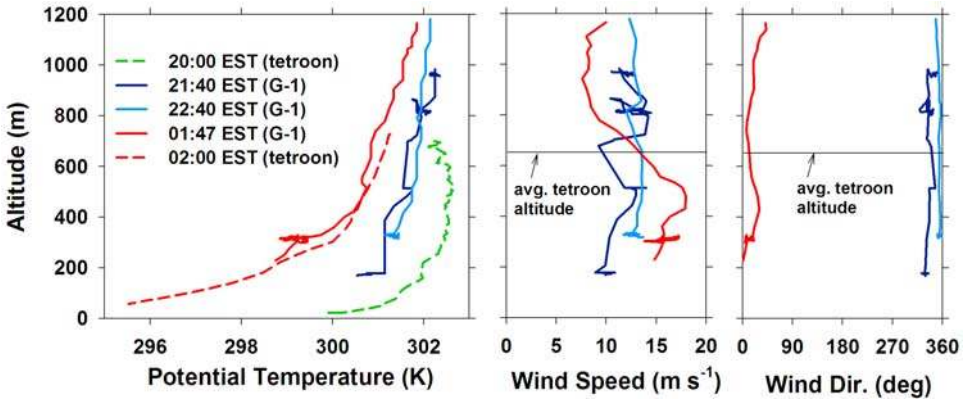

Figure 3. Vertical profiles of potential temperature, wind speed, and wind direction.

times for the four plume segments. In these calculations, the nocturnal jet was assumed to grow linearly in time between 2240 and 0200 EST. The resulting mean processing times (Δt) for the four plume segments were obtained as follows: A-high = 2.6 ± 0.1 h, A-low = 3.2 ± 0.2 h, B-low = 6.2 ± 0.2 h, and B-high = 7.2 ± 0.2 h, which are also indicated in Figure 2.

3.3. NO_x/NO_y Ratio and Odd Oxygen Budget

[24] Figure 6 shows the NO_x versus NO_y correlation for each of the four plume segments. The NO_x mixing ratio in the plume is expected to gradually decrease with time because of continued reaction with the residual O_3 and other reactants to form NO_3, N_2O_5, HNO_3, and other reactive nitrogen species such as nitrous acid (HONO), pernitric acid (HNO_4), organic nitrates (ONIT), and peroxy acyl nitrates (PAN). In the absence of dry deposition, the total measured NO_y mixing ratio, which includes NO_x, NO_3, $2N_2O_5$, HNO_3, HONO, HNO_4, PAN, and ONIT, is expected to remain constant. As a result the NO_x/NO_y ratio (i.e., the slope of NO_x versus NO_y correlation) is expected to gradually decrease with increasing processing time. However, the slope of the observed correlation remained fairly constant for all four plume segments. This unexpected behavior, as discussed in section 4, is attributed to a measurement artifact due to partial decomposition of NO_2 reservoirs (N_2O_5 and NO_3) in the chemiluminescence instrument, which led to between 12% and 74% overestimation of NO_2 and thereby fortuitously caused the NO_x/NO_y ratio to remain constant with time.

[25] The total odd oxygen budget analysis is useful for keeping track of rapid chemical cycling that takes place between O_3 and other members of the odd-oxygen family [*Jacob et al.*, 1996; *Brown et al.*, 2006a]:

$$[O_x] = [O_3] + [NO_2] + 2[NO_3] + 3[N_2O_5] + 1.5[HNO_3] + [HNO_4] + [PAN] + [ONIT] \quad (1)$$

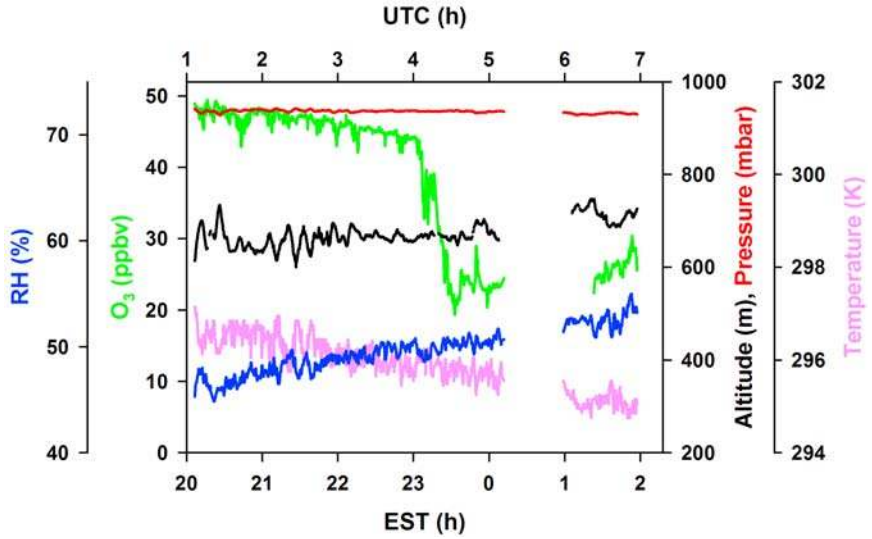

Figure 4. Tetroon-based O_3 and meteorological observations. The sudden drop of ~20 ppbv at 2300 EST could be due to a malfunction in the ozone sensor or due to the tetroon drifting into a markedly different plume layer. The latter seems less likely because the altitude fluctuations were minimal and no sudden changes were observed in RH when the O_3 mixing ratio rapidly decreased.

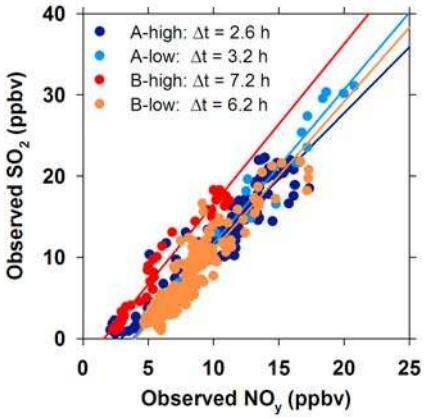

Figure 5. Correlation between SO_2 and NO_y in the Salem Harbor power plant plume segments sampled by the G-1 aircraft. The color code matches the one used in Figure 2.

The first two terms ($[O_3] + [NO_2]$) were measured directly. The remaining terms, which involve reactive nitrogen, can be estimated from the measured $[NO_y]$ by subtracting the measured $[NO_x]$. This difference, termed $[NO_z] = [NO_y] - [NO_2] - [NO]$, is then expected to consist of $[NO_3] + 2[N_2O_5] + [HNO_3] + [HONO] + [HNO_4] + [ONIT] + [PAN]$. However, if NO_z in the power plant plume segments is dominated by N_2O_5, HNO_3, or both, then the total odd oxygen budget in the plume with respect to the background can be approximated as

$$[O_x] = [O_3] + \Delta[NO_2] + 1.5\Delta[NO_z], \quad (2)$$

where Δ denotes the difference between the mixing ratio in the plume and in the nearby background air. Thus, if the total odd oxygen is conserved, then according to equation (2) the O_x mixing ratios in the plume should be equal to the O_3 mixing ratio in the background air.

[26] Figure 7 shows plots of O_3 versus NO_y and O_x versus NO_y in the four plume segments. As expected, O_3 is anticorrelated with NO_y due to titration by NO and subsequent reaction with NO_2. However, the total odd oxygen O_x, as estimated from equation (2), remains fairly constant with increasing NO_y in all four plume segments. This constancy in O_x across the plume segments at any given time indicates that the total odd oxygen atoms were largely conserved in the plume with respect to the nearby background values. The estimated overcounting of O_x due to the NO_2 measurement artifact ranged between 0.1 and 2.8 ppbv, which is relatively small compared to the total O_x budget (50–65 ppbv) and can be ignored in this analysis. The variation in the mean O_x values between the different plume segments is attributed to spatial gradients in O_3 concentrations in the background air into which the power plant emissions were injected. Conservation of odd oxygen not only serves as an important check on the self-consistency of the O_3, NO_2, and NO_y measurements but also suggests that the NO_z in the plume segments is mostly composed of N_2O_5, HNO_3, or both. The results from this exercise are used in section 4 to initialize a Lagrangian box model for investigating the rate of heterogeneous hydrolysis of N_2O_5.

3.4. Volatile Organic Compounds (VOCs)

[27] An analysis of canister samples yielded observations of 114 individual VOCs (20 s averages). As shown in Figure 2, five canister samples were collected during the first G-1 flight. While none of the canister sample locations fall precisely in the selected plume segments, canisters V3, V4, and V5 contain evidence of the Salem power plant emissions as the G-1 intercepted the plume near the A-low segment on the return leg. Figure 8 shows correlations of selected VOCs with NO_y mixing ratios from these three canisters. Coal- and residual oil-fired power plants may emit a wide variety of VOCs at very small levels due to incomplete combustion and from liquid fuel storage and use, although very little information exists on such emissions in the literature. Positive correlations could be seen between power plant NO_y and some VOCs such as toluene, acetylene, and propane while biogenic isoprene and NO_y were anticorrelated. The isoprene levels in the background air were about 0.3 ppbv while less than 0.05 ppbv was observed inside the plume. Other biogenic VOCs such as α-pinene, β-pinene, limonene, camphene, myrcene, etc. were less than 0.005 ppbv or below the detection limit in the canister samples, both within and outside the power plant plume. Lower concentrations of isoprene in the plume are attributed to its rapid reaction with the elevated levels of NO_3. This phenomenon is investigated further with model calculations in section 4. It is also possible that modest amounts of urban emissions of NO_y and VOCs were mixed together with power plant emissions since the Salem Harbor power plant is situated in the Salem urban area. However, based on the correlations of SO_2 versus NO_y and the slopes of the regression fits shown in Figure 5 and discussed in section 3.2, it appears that the excess NO_y (above background levels) was emitted from the power plant. Never-

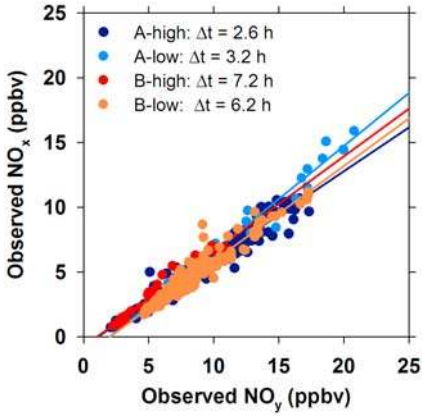

Figure 6. Scatterplot of NO_x versus NO_y in the Salem power plant plume segments. The NO_x/NO_y ratio (i.e., the slope of this correlation) is expected to decrease with time, increasing processing time at night, but note that the slopes of the observed correlations seem to remain fairly constant for processing times ranging from 2.6 to 7.2 h. The color code matches the one used in Figure 2.

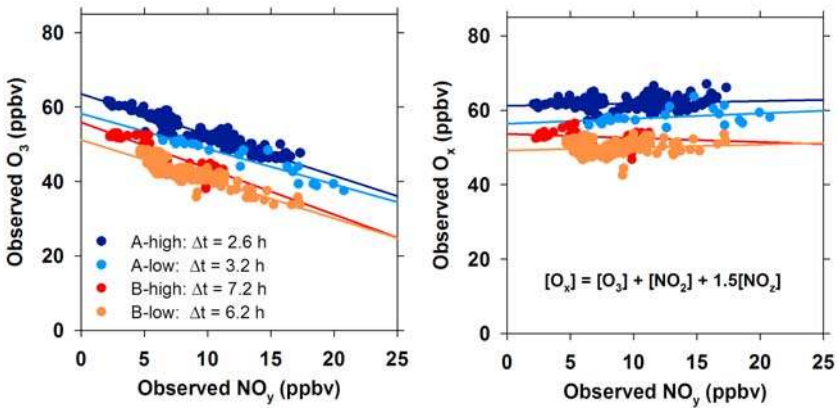

Figure 7. Scatterplots of O_3 versus NO_y and total odd oxygen O_x versus NO_y. As expected for nighttime emissions of NO, O_3 is anticorrelated with NO_y. Also note that O_x remains fairly constant with increase in NO_y, implying that the total odd oxygen atoms were largely conserved in the plume segments as expected. The color code matches the one used in Figure 2.

theless, the presence of small amounts of NO_y of urban area origin possibly mixed with NO_x emitted from the power plant should not affect the analysis and interpretation of the measurements presented in the rest of this paper.

3.5. Aerosol Concentration and Composition

3.5.1. Number Size Distribution

[28] A condensation particle counter (CPC) provided a 1 min averaged total number concentration of particles greater than 10 nm in diameter while a 15-channel passive cavity aerosol spectrometer probe (PCASP) provided a 1 s averaged particle number size distribution from 100 to 3000 nm diameter range. One-minute averaged particle number size distributions between 5 and 500 nm were also measured with a twin scanning electrical mobility spectrometer (TSEMS) [*Buzorius et al.*, 2004], which consists of one short differential mobility analyzer (DMA) and one long DMA operating in parallel.

[29] Figure 9 shows the CPC and total PCASP number concentrations and SO_2 mixing ratio along the four power plant plume segments. The CPC number concentrations were an order of magnitude higher than the total PCASP number concentrations, indicating that the number concentrations were dominated by ultrafine particles (<100 nm diameter). Furthermore, the CPC number concentrations were correlated with SO_2 in all four plume segments while the total PCASP number concentrations appear to be correlated with SO_2 only in the A-high and B-high plume segments. The total PCASP number concentrations in the A-low and B-low plume segments were relatively high, uniform, and uncorrelated with SO_2.

[30] Figure 10 shows a comparison of TSEMS size-distributed number concentrations observed within the power plume segment at A-high and just outside of it in the background air at the same altitude. The concentration of particles between 5 and 20 nm diameter (i.e., roughly the nucleation mode) in the plume were four times higher than that in the background air. These results clearly indicate that the Salem Harbor power plant was a significant source of ultrafine particles, especially the nucleation-mode particles, which would have formed by gas-to-particle conversion of SO_3/H_2SO_4 vapors directly emitted from the power plant [*Mueller and Imhoff*, 1994; *Srivastava et al.*, 2004; *Cichanowicz*, 2007].

3.5.2. Aerosol Mass Spectrometer Composition

[31] The Aerodyne Q-AMS measured nonrefractory aerosol components (sulfate, nitrate, chloride, ammonium, and total organics) for particles with vacuum aerodynamic diameters between 60 and 600 nm with 100% transmission efficiency [*Jayne et al.*, 2000]. Figure 11 shows particulate sulfate and organic mass concentrations plotted against SO_2 for the four plume segments. To obtain a high signal-to-noise ratio, the Q-AMS was operated on a 30 s cycle during the first G-1 flight and on a 120 s cycle during the second flight. As result, only a few data points were obtained within the power plant plume segments, especially during the second flight. Nevertheless, a number of interesting features are revealed in these plots.

[32] First, sulfate was positively correlated with SO_2 (except in the B-low plume segment), with sulfate mass at the peak of the plumes ranging between 0.5 and 1.5 $\mu g\ m^{-3}$

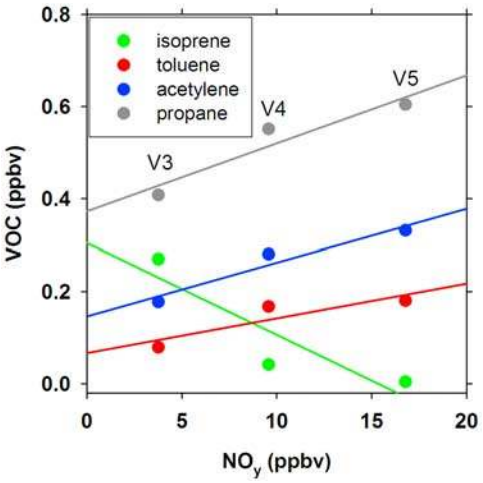

Figure 8. Correlations of selected canister VOCs with NO_y.

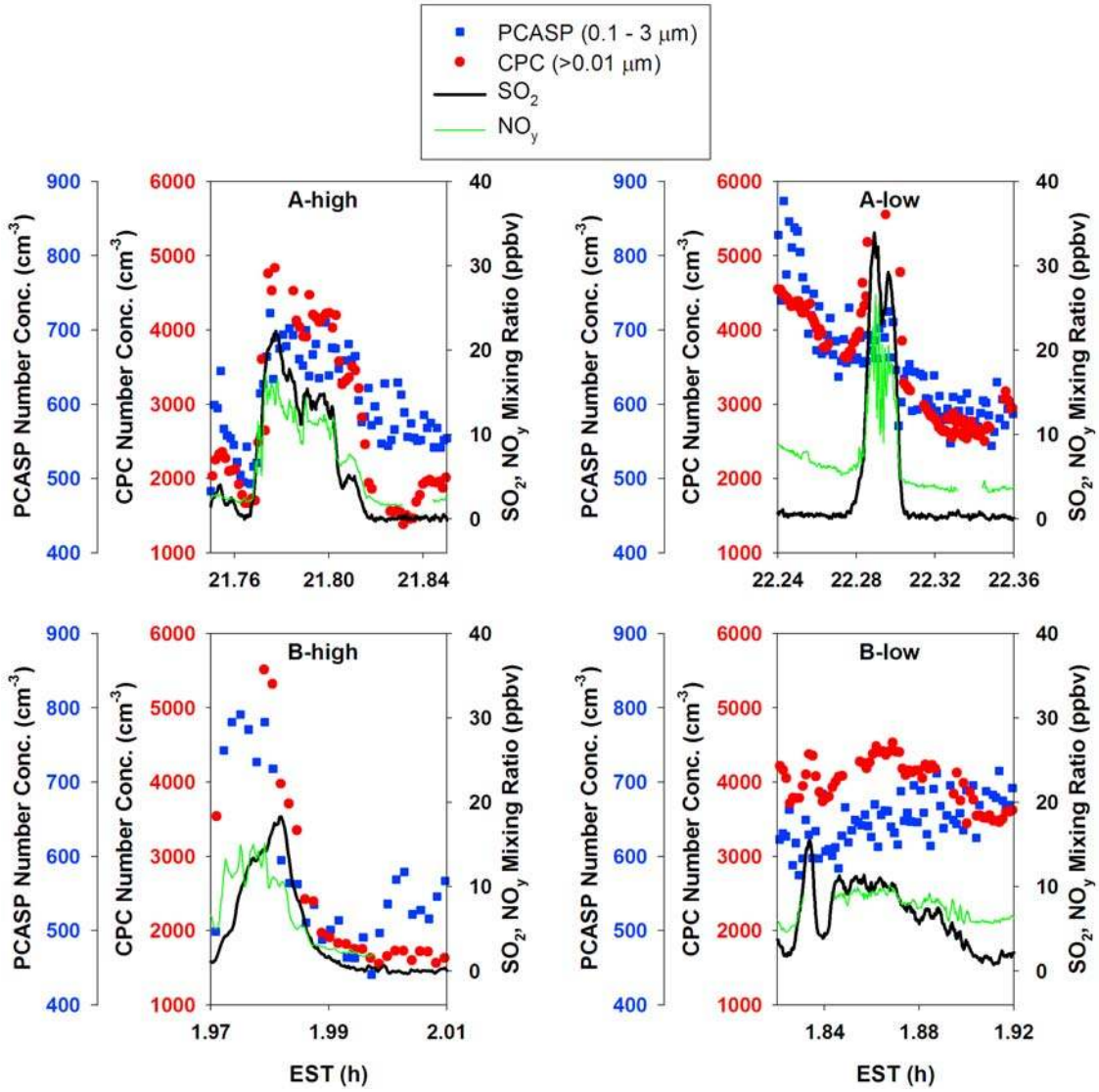

Figure 9. Total PCASP (0.1–3 μm) and CPC (>0.01 μm) aerosol number concentrations, SO_2, and NO_y mixing ratios along the four power plant plume segments.

in excess of the background value of ~1.5 μg m^{-3}. These results are consistent with the total PCASP and CPC versus SO_2 correlations shown earlier, and they support the notion of new particle formation from SO_3/H_2SO_4 vapors directly emitted from the power plant. Oxidation of SO_2 by OH radicals to form H_2SO_4 would be very slow at night and could not account for the observed sulfate excesses in the plume. While the direct emissions of SO_3/H_2SO_4 were not reported in the inventory for the Salem Harbor power plant, we estimated that they were ~1% (by mole) of the SO_2 emissions, which is within the range of values determined for several coal- and fuel oil–fired boilers [*Cichanowicz*, 2007].

[33] Second, organic aerosol (OA) mass was two to three times higher than sulfate mass, and a weak but distinct correlation was also seen between OA mass and SO_2 (except in the B-low plume segment). For instance, in both A-low and A-high plume segments, the OA mass at the peak of the plume was ~1 μg m^{-3} higher than the nearby background air

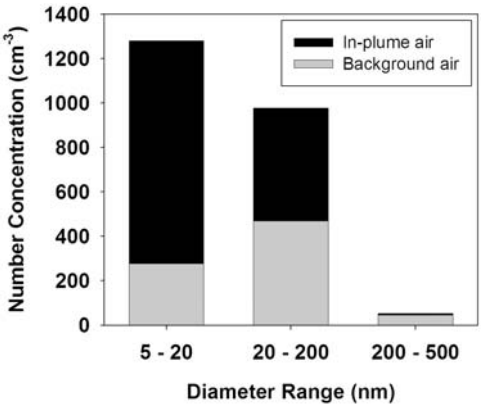

Figure 10. Size-distributed number concentrations observed within the power plume segment at A-high and just outside of it in the background air at the same altitude.

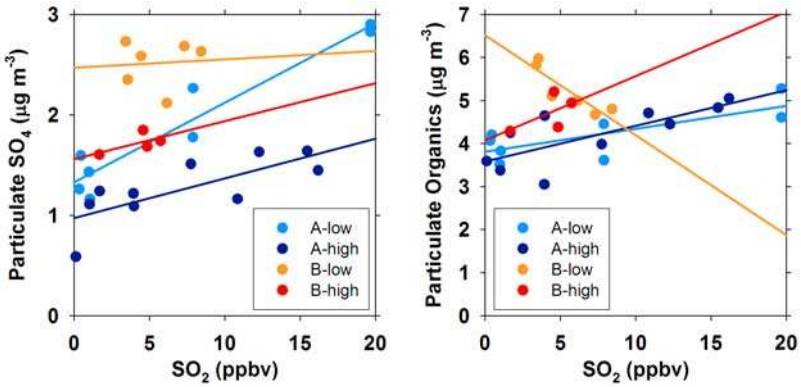

Figure 11. Particulate sulfate and organic mass concentrations (measured by the Q-AMS) as a function of SO_2 mixing ratios in the four power plant plume segments.

value of ~4 μg m^{-3}. Data on primary OA emission from coal-fired power plants is rather scarce in the literature, although some evidence exists for small amounts of primary OA emissions from no. 2 distillate fuel oil–fired boilers [*Rogge et al.*, 1997]. Primary OA particles, if they were emitted from the Salem Harbor power plant, would likely have also contained traces of fly ash minerals such as oxides of Al, Fe, Na, K, Ca, Si, V, etc. [*Goldstein and Siegmund*, 1976; *Damle et al.*, 1982; *Querol et al.*, 1996]. However, as discussed in section 3.6.3, X-ray microanalysis of individual particles in several in-plume and background air TRAC samples showed no evidence of any fly ash elements whatsoever. It therefore appears that primary aerosol particles were efficiently removed by the electrostatic precipitators at the Salem Harbor power plant.

[34] A more plausible explanation for the observed excess OA mass in the power plant plume is the formation of SOA such as low-volatility organic nitrates from isoprene oxidation with NO_3 [*Barnes et al.*, 1990; *Shepson et al.*, 1996; *Starn et al.*, 1998; *Ng et al.*, 2008]. About 65% conversion of the observed 0.3 ppbv of isoprene in the background air to low-volatility isoprene nitrates can potentially account for the observed excess OA of 1 μg m^{-3} in the plume. SOA consisting of organosulfates could also have been formed by heterogeneous reactions between acidic sulfate particles and biogenic VOCs (such as isoprene and monoterpenes) as well as their photooxidation products (such as pinonaldehyde and dihydroxyepoxides) that likely remained in the residual layer from the preceding afternoon [*Liggio and Li*, 2006; *Liggio et al.*, 2007; *Paulot et al.*, 2009]. Oxidation of isoprene with NO_3 radicals in the presence of acidic sulfate particles could have also led to the formation of nitroxy organosulfate SOA [*Surratt et al.*, 2008].

[35] If the NO_3 radical-initiated oxidation of isoprene and other trace organic gases indeed contributed to SOA formation in the plume, then the observed particulate nitrate would be in the form of organic nitrate. Support for the presence of organic nitrates comes from the plots of particulate nitrate versus NO_y and particulate nitrate versus particulate $[NH_4]/[SO_4]$ molar ratio for the four plume segments (Figure 12). Particulate nitrate concentrations were rather small (<0.5 μg m^{-3}) but weakly correlated with NO_y. In the plot of particulate nitrate versus $[NH_4]/[SO_4]$ molar ratio, we found that most of the nitrate-containing aerosol particles were highly acidic as inferred from the bulk $[NH_4]/[SO_4]$ molar ratios of less than 2. Also, there was no systematic dependence of nitrate concentrations on particle acidity. The equivalent gas-phase mixing ratio of the highest particulate nitrate concentration observed was less than 0.2 ppbv, which constitutes a rather negligible fraction of the

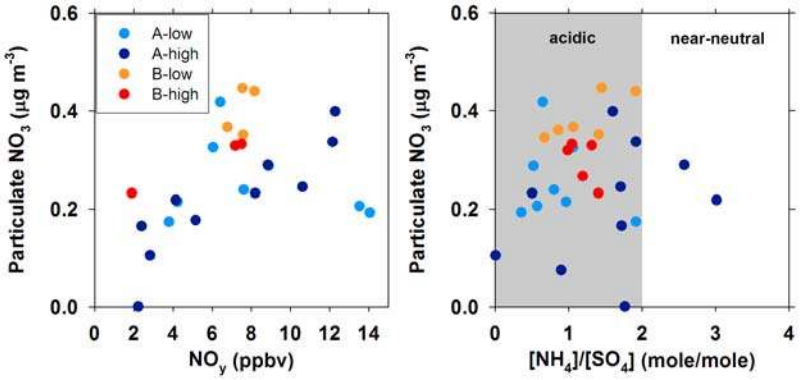

Figure 12. Particulate nitrate versus NO_y and particulate nitrate versus $[NH_4]/[SO_4]$ molar ratio for the four power plant plume segments.

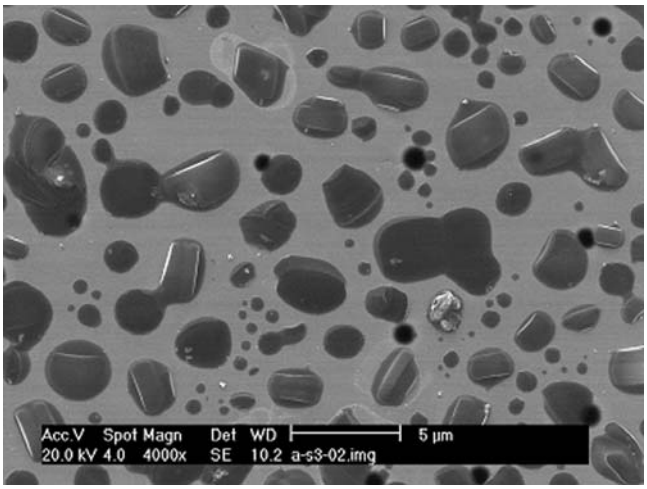

Figure 13. Typical SEM image of aerosol particles collected within the plume (location P1 in Figure 2).

total NO_y budget. But the fact that the particulate nitrate was not neutralized by NH_4^+, and that its concentration was insensitive to acidity, suggests that it was in the form of organic nitrates rather than nitrate ion. It should be noted that the inferred maximum level of 0.2 ppbv of organic nitrates is 66% of the 0.3 ppbv isoprene available in the background air, which is consistent with the mass balance argument for excess OA presented in the preceding paragraph. The organic nitrate hypothesis was further scrutinized by calculating the equilibrium gas-phase HNO_3 mixing ratio over such acidic particles, assuming that the observed particulate nitrate was in the form of inorganic nitrate ion. The online version of the Aerosol Inorganics Model (AIM II/Comprehensive Calculation, see http://www.aim.env.uea.ac.uk/aim/aim.php) [*Wexler and Clegg*, 2002] was used to perform the equilibrium calculation for a representative plume aerosol sample with $[NH_4]/[SO_4]$ molar ratio of unity, containing $[SO_4^{2-}] = 0.016$ μmol m^{-3} (= 1.5 μg m^{-3}), $[NH_4^+] = 0.016$ μmol m^{-3} (= 0.29 μg m^{-3}), and $[NO_3^-] = 0.005$ μmol m^{-3} (= 0.3 μg m^{-3}). The value of $[H^+]$ concentration required as input into the model was calculated from the electroneutrality condition as $[H^+] = 2[SO_4^{2-}] + [NO_3^-] - [NH_4^+] = 0.021$ μmol m^{-3}. The input ambient temperature and relative humidity were 298 K and 65%, respectively. With these constraints, the predicted equilibrium gas-phase HNO_3 mixing ratio was 3820 ppbv. This value is unreasonably high since the observed total NO_y mixing ratios were <15 ppbv. Other similar aerosol compositions also resulted in HNO_3 mixing ratios greater than 1000 ppbv. Therefore, it follows that most of the observed particulate nitrate was likely in the form of organic nitrate rather than inorganic nitrate ion.

[36] Additional insights into the mixing state of aerosol particles and the presence of organosulfates and sp^2 hybridized C = C bonds in the organic aerosol was obtained from microspectroscopic analyses of the collected particle samples, which is discussed next.

3.5.3. Microscopy and Microspectroscopic Analyses

[37] A few of the particle samples collected by TRAC were selected for microscopy and microspectroscopy studies. The sampling times and locations are indicated by the numbered pink hexagons (P0, P1, and P2) in Figure 2. Each TRAC sample consists of particles collected over a 2 min period. The P0 sample was taken in the background air while the P1 and P2 samples were taken in the plume segments at A-low and B-low, respectively. Figure 13 shows a typical scanning electron microscopy (SEM) image of particles collected within the plume at location P1. Microscopy analysis of samples from the other two locations (P0 and P2) showed no major difference in particle images. X-ray microanalysis of individual particles indicated the presence of carbon, oxygen, and sulfur, revealing the dominant presence of internally mixed organic and sulfate particles within the power plant plume as well as in the background air. However, no evidence was found for any fly-ash-type materials within the plume, suggesting that all primary aerosol particles were efficiently filtered out by the electrostatic precipitators at the power plant.

[38] Subsequent scanning transmission X-ray microscopy (STXM) combined with near-edge X-ray absorption fine structure spectroscopy (NEXAFS) analysis of these samples was performed at the Advanced Light Source, Lawrence Berkeley National Laboratory, at beamline 11.0.2. This technique provides detailed information on the carbon [*Hopkins et al.*, 2007a, 2007b; *Maria et al.*, 2004; *Michelsen et al.*, 2007; *Takahama et al.*, 2008; *Tivanski et al.*, 2007; *Moffet et al.*, 2009], sulfur [*Hopkins et al.*, 2008], and metal bonding within aerosols [*Moffet et al.*, 2008; *Takahama et al.*, 2008]. For this study, the carbon *K* edge (280–320 eV), oxygen *K* edge (525–550 eV), nitrogen *K* edge (385–430 eV) and sulfur *L* edge (167–176 eV) were examined. NEXAFS spectra of particles at the three locations (P0, P1, and P2) were recorded at the carbon and sulfur (168–176 eV) *L* edges.

[39] Figure 14 displays (left) the characteristic NEXAFS carbon *K*-edge and (right) the corresponding sulfur *L*-edge spectra. The carbon and sulfur spectra were pre-edge background subtracted and normalized to the 320 and 172.1 eV intensities, respectively. In contrast to most atmospheric particulate samples examined in other field campaigns, the aerosol spectra obtained for all the samples in this study were extremely homogeneous both within individual particles and from particle to particle. The spectra were therefore averaged over ~50 individual particles in each sample. All carbon *K*-edge spectra displayed a well-defined peak at 285.15 eV which was unambiguously assigned to a carbon $1S \rightarrow 1\pi^*$ aromatic C = C transition [*Hopkins et al.*, 2007b]. Organic aerosols containing sp^2 hybridization (C = C double bonds) have been observed during several other field studies around the world [*Takahama et al.*, 2007]. While the origin of these C = C double bonds is not clear, one possible way they could form within organic aerosols is via aldol reaction followed by a dehydration step to form "humic-like" polyconjugated oligomeric compounds (i.e., containing alternating single and double bonds) [e.g., *Nozière et al.*, 2007, 2009].

[40] All sulfur *L*-edge spectra displayed three distinct peaks, which can be assigned as follows: a peak at 170.9 eV, $S\ 2p_{3/2} \rightarrow 1\pi^*$; a peak at 172.1 eV, $S\ 2p_{1/2} \rightarrow 1\pi^*$; and a peak at 172.9 eV, $S\ 2p_{3/2} \rightarrow 2\pi$ [*Hopkins et al.*, 2008]. These spectral contours and the peak positions are indicative of the sulfate bonding [*Hopkins et al.*, 2008]. Although this

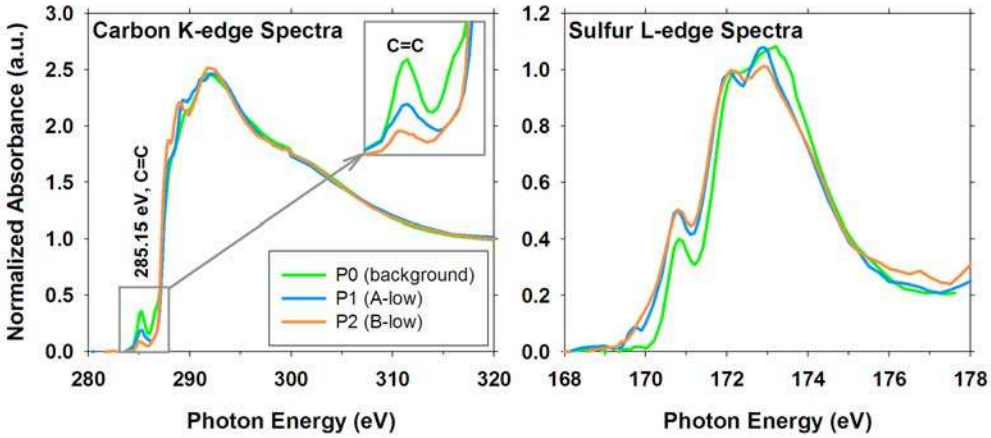

Figure 14. Representative (left) carbon *K*-edge and (right) sulfur *L*-edge NEXAFS spectra of particles sampled at locations P0, P1, and P2 (see Figure 2). Decreasing intensity of the normalized 285.15 eV peak in the carbon *K*-edge spectra from locations P0 to P2 indicates consumption of C = C bonds in particles sampled along the plume trajectory.

previous study indicated that the sulfur *L*-edge NEXAFS spectra do not distinguish between different types of sulfates, STXM images at both carbon and sulfur absorption edges indicate a homogeneous distribution within particles containing sulfur and carbon. It has been previously observed that nitrogen *K*-edge spectra of inorganic sulfur (i.e., ammonium sulfate) were very sensitive to X-ray exposure, which resulted in distinct changes in the chemical bonding (growth of a peak at 401 eV). Such sensitivity and spectral changes at the nitrogen *K* edge were not observed in the present samples (spectra are not shown). We therefore tentatively assign some of the observed sulfate bonding to that of an organosulfate. Again, the formation of organosulfates from biogenic VOCs in the presence of acidic sulfate particles is consistent with the results from a number of laboratory studies [*Liggio and Li*, 2006; *Liggio et al.*, 2007; *Surratt et al.*, 2008].

[41] The C = C peak at 285.15 eV of the carbon *K*-edge NEXAFS spectra displayed a decrease in percent of sp^2 hybridized C = C bonds in the particles as a function of processing time in the plume. The processing time for the background particles is assumed to be zero. The extent of the sp^2 hybridization can be estimated relative to the highly oriented pyrolytic graphite (HOPG), for which 100% sp^2 hybridization is assumed [*Hopkins et al.*, 2007a, 2007b; *Michelsen et al.*, 2007]. To quantify the observed decrease for these samples, the peak area of the aromatic C = C peak at 285.15 eV was normalized to the area of the spectrum over the energy range 280–320 eV for each sample. This ratio was then compared with the ratio obtained for the HOPG. The calculated percent of sp^2 hybridization values for the locations P0, P1, and P2 are about 8%, 4%, and 1.6%, respectively. The decrease in the percent of sp^2 hybridization from 8% at P0 to <2% at P2 indicates the consumption of C = C bonds in the particles sampled along the plume trajectory (Figure 15). One possible explanation is a heterogeneous reaction between elevated levels of the NO_3 radicals present in the power plant plume with the C = C bonds. Such reactions could also form small amounts of organic nitrates [e.g., *Moise et al.*, 2002; *Hung et al.*, 2005; *Docherty and Ziemann*, 2006; *Gross and Bertram*, 2009]. We now turn to a model analysis of the aircraft and tetroon observations to gain further insight into the chemical processing of O_3, NO_x, and VOCs and the efficiency of the N_2O_5 heterogeneous hydrolysis reaction in the power plant plume.

4. Constrained Plume Modeling (CPM) Analysis of N_2O_5 Hydrolysis

[42] As mentioned earlier, the overall rate and efficiency with which NO_x is converted to HNO_3 at night is of great interest, because at dawn the residual NO_3 and N_2O_5 can photolyze or dissociate back to NO_x and subsequently produce O_3 in the presence of VOCs. One of the key reactions that convert NO_x to HNO_3 at night is the heterogeneous hydrolysis of N_2O_5 on an aerosol surface. The sequence of

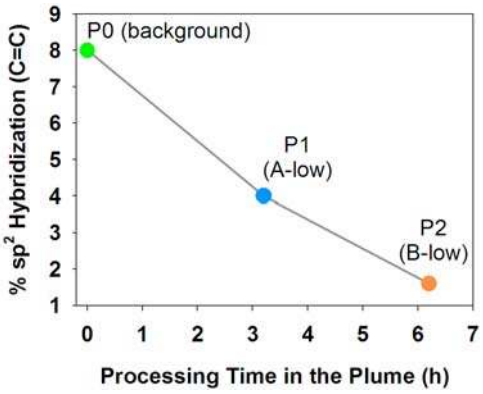

Figure 15. Evolution of percent sp^2 hybridization (C = C) as a function of processing time in the power plant plume. P0 corresponds to the background sample while P1 and P2 are in-plume samples at A-low and B-low plume segments, respectively, as indicated in Figure 2.

reactions leading to N_2O_5 hydrolysis is summarized as follows [*Brown et al.*, 2003, 2004]:

$$O_3 + NO \rightarrow NO_2 + O_2, \quad (3)$$

$$O_3 + NO_2 \rightarrow NO_3 + O_2, \quad (4)$$

$$NO_3 + NO_2 \Leftrightarrow N_2O_5, \quad (5)$$

$$N_2O_5 + H_2O \xrightarrow[\gamma(N_2O_5)]{\text{het.}} 2HNO_3. \quad (6)$$

The N_2O_5 uptake coefficient $\gamma(N_2O_5)$ in equation (6) is a reaction probability, which is defined as the fraction of gas-particle collisions of one molecule of gaseous N_2O_5 that results in net hydrolysis to produce two molecules of HNO_3. From the definition of $\gamma(N_2O_5)$, it follows that the net loss rate of N_2O_5 can be expressed as [*Jacob*, 2000]

$$\frac{d[N_2O_5]}{dt} = -k[N_2O_5], \quad (7)$$

$$k = 4\pi \sum_i N_i R_{p,i}^2 \left[\frac{R_{p,i}}{D_g} + \frac{4}{v\gamma(N_2O_5)}\right]^{-1}, \quad (8)$$

where k (s^{-1}) is the first-order mass transfer coefficient that is a function of gas-phase diffusivity D_g ($cm^2\ s^{-1}$) of N_2O_5, mean molecular speed v ($cm\ s^{-1}$) of N_2O_5 in the gas phase, N_2O_5 uptake coefficient $\gamma(N_2O_5)$, mean particle radius $R_{p,i}$ (i = size bin), and number concentration [N_i (cm^{-3})] of particles of mean radius $R_{p,i}$.

[43] Laboratory studies of N_2O_5 hydrolysis on pure water droplets and aqueous inorganic aerosols have shown values of $\gamma(N_2O_5)$ in the range of 0.005 at low RH to 0.09 at high RH [*Mozurkewich and Calvert*, 1988; *Van Doren et al.*, 1990; *Msibi et al.*, 1994; *Hu and Abbatt*, 1997; *Wahner et al.*, 1998; *Kane et al.*, 2001; *Hallquist et al.*, 2003; *Thornton and Abbatt*, 2005]. Laboratory studies of N_2O_5 uptake on some organic aerosols have also shown small values for $\gamma(N_2O_5)$ ranging from 0.0005 to 0.002 at low RH and as high as 0.03 at moderate RH (50–70%) [*Thornton et al.*, 2003; *Bertram and Thornton*, 2009]. Moreover, reductions in $\gamma(N_2O_5)$ by a factor of 3 to more than an order of magnitude were observed when certain organic coatings were present on inorganic particles [*Folkers et al.*, 2003; *Thornton and Abbatt*, 2005; *Badger et al.*, 2006; *McNeill et al.*, 2006]. Laboratory studies have also shown a reduction in $\gamma(N_2O_5)$ in the presence of nitrate ion (NO_3^-) in aqueous aerosols [*Wahner et al.*, 1998; *Mentel et al.*, 1999; *Hallquist et al.*, 2003; *Bertram and Thornton*, 2009].

[44] Based on the constrained steady-state analysis of aircraft observations of O_3, NO_3, and N_2O_5 in urban and power plant plumes in the northeastern United States, *Brown et al.* [2006b] estimated negligibly small values for $\gamma(N_2O_5)$ (<0.001) in the presence of near-neutral aerosol particles (i.e., $[NH_4]/[SO_4]$ molar ratios ~2) with organic/sulfate mass ratios between 0.5 and 1. On the other hand, a relatively high value of $\gamma(N_2O_5) = 0.017$ was estimated in the presence of acidic aerosol particles ($[NH_4]/[SO_4]$ molar ratios ~1) that had organic/sulfate mass ratios of ~0.2. These laboratory and field measurements show a wide range of values for $\gamma(N_2O_5)$ that appear to be strongly dependent on aerosol composition, relative humidity, and particle phase state. It generally appears that highly hydrated, acidic aerosols lead to large values for $\gamma(N_2O_5)$ while high organic/sulfate ratios and nitrate ion–containing aerosols lead to low values for $\gamma(N_2O_5)$.

[45] As discussed in the section 3.5.2, the aerosol particles in the four plume segments were largely acidic ($[NH_4]/[SO_4] < 2$) with organic/sulfate mass ratios of 2–3. These particles were likely deliquesced at the ambient RH of ~60–70%, and the small but non-negligible amounts of particulate nitrate observed were likely in the form of organic nitrate. Based on the literature summarized above, $\gamma(N_2O_5)$ for such particles and conditions could range from negligibly small (<0.001) up to 0.03. Here we employ a CPM analysis approach to interpret the tetroon and aircraft observations in the power plant plume to estimate the value of $\gamma(N_2O_5)$ that is pertinent to the conditions observed in this study.

[46] In the CPM approach, a Lagrangian gas-aerosol box model is initialized using the available ground and/or aircraft observations at or near the plume emission source. The box model is then integrated forward in time, taking into account the changes in species concentrations inside the box due to emissions, gas-phase reactions, gas-particle interactions, dry deposition, and dilution along an observed or predicted trajectory. The predicted species concentrations are then evaluated against observations in the plume at increasing downwind distances with estimated processing times since initialization [e.g., *Zaveri et al.*, 2003; *Real et al.*, 2008].

[47] In this study, we use the comprehensive gas-aerosol model MOSAIC (Model for Simulating Aerosol Interactions and Chemistry) [*Zaveri et al.*, 2008] in a Lagrangian box-model framework. We initialize and constrain the model with several key observations to estimate a value for $\gamma(N_2O_5)$ such that the predicted evolution of O_3 and NO_x mixing ratios in the power plant plume are consistent with their observed counterparts.

4.1. Model Description and Inputs

[48] MOSAIC employs comprehensive treatments for aerosol chemistry, thermodynamics (phase state and water content), dynamic gas-particle partitioning, and other microphysical processes [*Zaveri et al.*, 2005a, 2005b, 2008]. MOSAIC employs the gas-phase photochemical mechanism Carbon Bond Mechanism (CBM-Z) [*Zaveri and Peters*, 1999], which contains all the standard trace gas reactions typically represented in air quality models. The model includes the heterogeneous hydrolysis of N_2O_5 on an aerosol surface and allows the user to set the value for $\gamma(N_2O_5)$. The Lagrangian box-model version of MOSAIC also includes chemical reactions and dry deposition and allows for dilution and vertical entrainment in a developing boundary layer as described elsewhere [*Zaveri et al.*, 2003].

[49] In the present application, vertical entrainment and dry deposition were ignored since the plume segments are assumed to start within the nocturnal residual layer that is effectively decoupled from the stable marine layer (based on the potential temperature profiles shown in Figure 3). The Lagrangian box model is initialized at the Salem Harbor

Table 1. List of CBM-Z Model Species, Their Background Mixing Ratios, and Estimated Emission Factors (f_{VOC})

No.	Species Name or Class	CBM-Z Species	Background Mixing Ratio (ppbv)	f_{PVOC}
1	Nitrogen dioxide	NO_2	0.4	
2	Nitric acid[a]	HNO_3	0.5–0.75	
3	Peroxy acyl nitrate[a,b]	PAN	1–1.75	
4	Methane	CH_4	1800	
5	Ethane	C_2H_6	1	0.03
6	Paraffin carbon (alkanes)	PAR	3.3	0.3
7	Ethylene	ETH	0.5	0.018
8	Terminal olefins	OLET	0.13	0.006
9	Toluene	TOL	0.15	0.01
10	Xylene	XYL	0.004	0.004
11	Isoprene	ISOP	0.3	

[a]Background NO_z was 1.5–2.5 ppbv of which ~70% was assumed as PAN and the remaining as HNO_3 based on the aircraft measurements in aged background air over central Massachusetts during summer [*Berkowitz et al.*, 1998].

[b]When initializing PAN in the model, the acyl peroxy radicals are also set such that they are in equilibrium with the specified PAN and observed NO_2 at a given temperature.

power plant for each G-1 aircraft measurement point (1 s average; total 753 points) in the four plume segments as follows:

$$[\text{aerosol size dist}]_0^{\text{plume}} = [\text{aerosol size dist}]_{\text{G-1}}^{\text{plume}}, \quad (9)$$

$$[\text{NO}]_0^{\text{plume}} = [\text{NO}_y]_{\text{G-1}}^{\text{plume}} - [\text{NO}_z]_{\text{G-1}}^{\text{bkg}}, \quad (10)$$

$$[\text{NO}_2]_0^{\text{plume}} = [\text{NO}_2]_{\text{G-1}}^{\text{bkg}}, \quad (11)$$

$$[\text{HNO}_3]_0^{\text{plume}} = 0.3[\text{NO}_z]_{\text{G-1}}^{\text{bkg}}, \quad (12)$$

$$[\text{PAN}]_0^{\text{plume}} = 0.7[\text{NO}_z]_{\text{G-1}}^{\text{bkg}}, \quad (13)$$

$$[\text{O}_3]_0^{\text{plume}} = [\text{O}_3]_{\text{G-1}}^{\text{plume}} + \left([\text{NO}_2]_{\text{G-1}}^{\text{plume}} - [\text{NO}_2]_{\text{G-1}}^{\text{bkg}}\right) + 1.5\left([\text{NO}_z]_{\text{G-1}}^{\text{plume}} - [\text{NO}_z]_{\text{G-1}}^{\text{bkg}}\right), \quad (14)$$

$$[\text{BVOC}]_0^{\text{plume}} = [\text{BVOC}]_{\text{G-1}}^{\text{bkg}}, \quad (15)$$

$$[\text{PVOC}]_0^{\text{plume}} = [\text{PVOC}]_{\text{G-1}}^{\text{bkg}} + f_{\text{VOC}}[\text{NO}]_0^{\text{plume}}, \quad (16)$$

where the subscript 0 refers to the initial concentration at the power plant and subscript G-1 refers to G-1 aircraft-based observation either at a point within a given plume segment (denoted by superscript "plume") or in the nearby background air (denoted by superscript "bkg"). The aerosol size distributions were based on the 15-channel PCASP data (100–3000 nm). BVOC and PVOC stand for biogenic VOC and power plant VOC, respectively. The coefficient f_{PVOC} for a given PVOC was determined from the slope of the VOC versus NO_y mixing ratio correlation obtained from canister data (as shown in Figure 8). A list of CBM-Z species, their background mixing ratios, and f_{PVOC} values are given in Table 1. Initial and background values for NO_3 and N_2O_5 were assumed to be zero.

[50] Since each box-model simulation (total 753) was initialized using the G-1 measurements at locations A and B, all the dilution that would occur between the point of emission and the G-1 measurement locations was implicitly taken into account right at the start of the simulation. The underlying assumption is that most of the fumigation and dilution of the power plant emissions with the background air in the nocturnal residual layer occurs within a few minutes after emission, with relatively slow dilution occurring because of the lack of turbulence as the plume is advected downwind through the course of the night. Emissions along the trajectory were ignored because of the over-ocean trajectory of the plume segments. After the box model was initialized for each point in a given segment, it was integrated forward for the estimated processing time (Δt) for that segment. The predicted O_3 and NO_2 mixing ratios were then evaluated against the observed values at their respective locations. In other words, the box model was initialized at the power plant (i.e., the point of emission) for each 1 s point in the A-high segment using the G-1 observations (as described earlier), integrated forward in time, and then evaluated using the O_3 and NO_2 observations in the A-high segment at its downwind location. Similarly, the box model was initialized at the power plant for each 1 s point in the A-low segment using the G-1 observations (as described earlier), integrated forward in time, and then evaluated using the O_3 and NO_2 observations in the A-low segment at its downwind location. The same procedure was carried out for the B-high and B-low segments. It is worth noting that the box model was not initialized at A, integrated forward in time, and evaluated at B.

4.2. Model Evaluation and Discussion

4.2.1. Evaluation Along the Tetroon Trajectory

[51] We first examine the time evolution of key species in the air parcel advected along the tetroon trajectory. The tetroon-borne ozone measurements indicate that the O_3 mixing ratio at ~670 m asl above the tetroon launch site was ~48 ppbv. Based on the total odd oxygen (O_x) analysis presented in section 3.3, the mean O_x mixing ratio at the tetroon altitude was ~58 ppbv, which is same as the O_3 mixing ratio just upwind of the Salem Harbor power plant (i.e., equation (14)). The difference between this initial value and the observed value of ~48 ppbv on board the tetroon must be due to titration by an initial NO mixing ratio of ~10 ppbv. The Lagrangian box model was thus initialized at the Salem Harbor power plant location with $[O_3]_0^{\text{plume}}$ = 58 ppbv, $[NO]_0^{\text{plume}}$ = 10 ppbv, $[SO_2]_0^{\text{plume}}$ = 20 ppbv, $[NO_2]_0^{\text{plume}}$ = 0.4 pbbv, $[PAN]_0^{\text{plume}}$ = 1.1 ppbv, and $[HNO_3]_0^{\text{plume}}$ = 0.4 ppbv. The initial isoprene and plume VOCs mixing ratios were estimated using the correlations given in Table 1. The initial aerosol size distribution was based on a representative aircraft observation corresponding to an SO_2 mixing ratio of 20 ppbv. A series of box-model simulations were performed with $\gamma(N_2O_5)$ values of 0.001, 0.01, and 0.1. Since the aerosol surface area used in these calculations only included particles between 100 and 3000 nm, the corresponding $\gamma(N_2O_5)$ values represent an

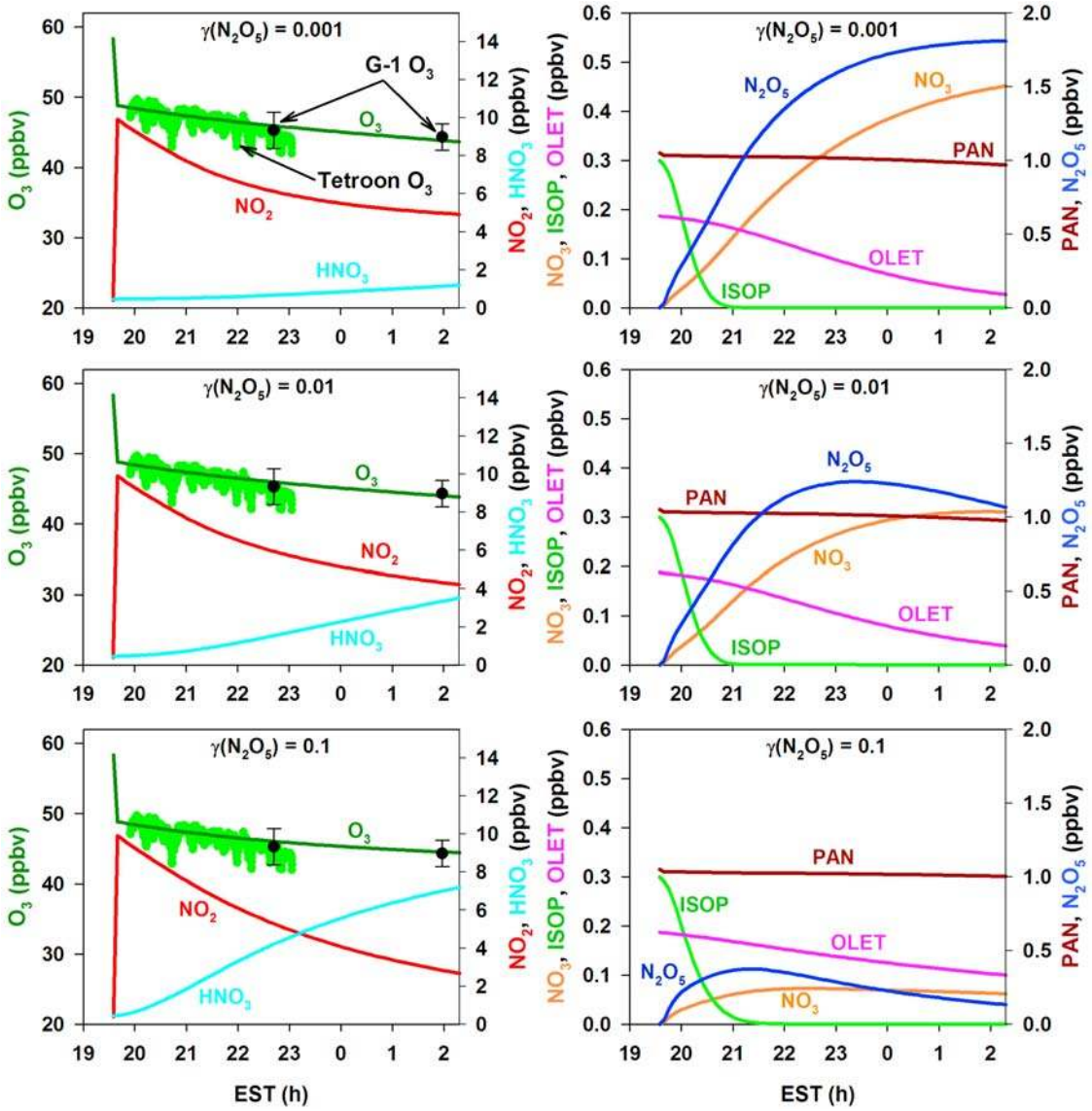

Figure 16. Predicted (lines) evolution of trace gases O_3, NO_2, HNO_3, NO_3, N_2O_5, PAN, ISOP (isoprene), and OLET (terminal olefins) along the tetroon trajectory for $\gamma(N_2O_5)$ values of (top) 0.001, (middle) 0.01, and (bottom) 0.1. O_3 observed on board the tetroon (solid green circles) and the G-1 aircraft (solid black circles) are also shown along with the predicted O_3. The G-1 aircraft O_3 mixing ratios (1 min averages with standard deviations) are at two instances (2240 and 0200 EST) when both the G-1 and tetroon were at similar altitudes and close to each other (3–7 km apart horizontally).

upper limit. The true values would be lower since they would scale to the total aerosol surface area.

[52] Figure 16 shows the predicted time evolution of various key trace gases along the tetroon trajectory for the three different values of $\gamma(N_2O_5)$. Figure 16 also shows comparisons of observed and predicted O_3, with the tetroon-based O_3 observations limited to the first 3 h of evolution due to the problem with the subsequent data, as explained in section 3.1. However, the plot includes O_3 observed on board the G-1 aircraft at two instances (2240 EST and 0200 EST), when both the G-1 and the tetroon were at similar altitudes and roughly 3–7 km apart. It can be seen that the predicted and observed O_3 mixing ratios are in excellent agreement. The sharp decrease in O_3 and the corresponding sharp increase in NO_2 in the beginning are due to the fast titration of O_3 with NO to give NO_2. The gradual decay in O_3 thereafter is largely due to the relatively slower $O_3 + NO_2$ reaction. It should be noted that O_3 decay is insensitive to the $\gamma(N_2O_5)$ value. However, the gradual decay in NO_2 depends not only on the $O_3 + NO_2$ reaction but also on its subsequent rapid and reversible reaction with NO_3 to form N_2O_5. For this reason, the loss rate of NO_2 and the formation rates of NO_3, N_2O_5, and HNO_3 are seen to be sensitive to the value of $\gamma(N_2O_5)$. Higher $\gamma(N_2O_5)$ values would result in lower NO_2, NO_3, and N_2O_5 mixing ratios and higher HNO_3 mixing ratios. In all cases, mod-

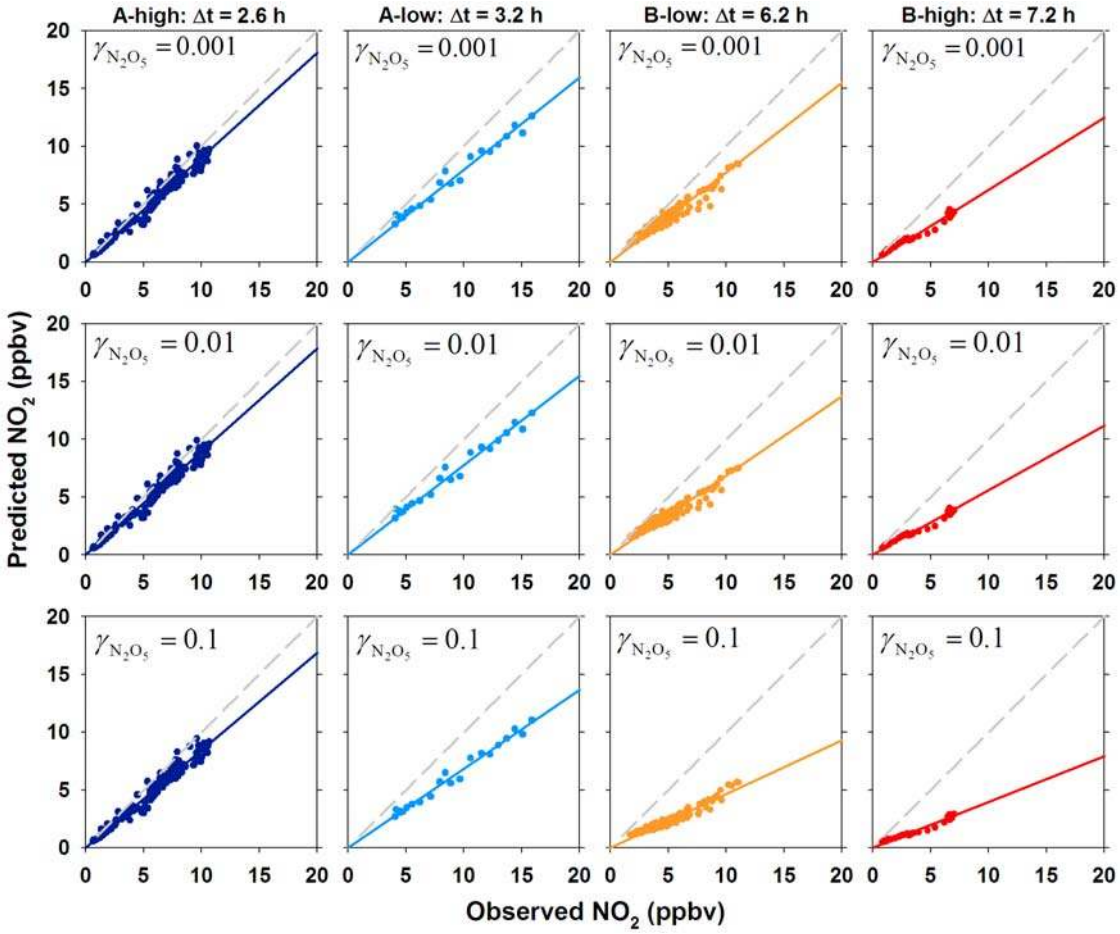

Figure 17. Predicted versus observed NO_2 mixing ratios for $\gamma(N_2O_5)$ values of 0.001, 0.01, and 0.1. Note that the predicted NO_2 mixing ratios are always lower than the observed values, and the underprediction progressively worsens with increasing processing time and with increasing $\gamma(N_2O_5)$ values.

eling results showed that isoprene was depleted within 2 h because of its high reactivity with NO_3. In contrast, the loss rate of less reactive olefins slowed down with increases in $\gamma(N_2O_5)$ because of the consequent reduction in the NO_3 radical concentrations, illustrating the coupling between N_2O_5 heterogeneous chemistry and homogeneous NO_3 chemistry.

4.2.2. Evaluation at the Four Plume Segments

[53] We now take advantage of the sensitivity of various trace gases, especially NO_2, to $\gamma(N_2O_5)$ in the CLM analysis of the four plume segments to estimate a value for $\gamma(N_2O_5)$ that is consistent with the observations presented in section 3. To examine the effect of the heterogeneous hydrolysis reaction on the evolution of O_3 and NO_2 mixing ratios, a series of simulations was carried out with $\gamma(N_2O_5)$ values of 0.001, 0.01, and 0.1. The predicted and observed O_3 mixing ratios were found to be in excellent agreement for each of the four plume segments for all three values of $\gamma(N_2O_5)$, indicating that the heterogeneous hydrolysis reaction had a negligible effect on the evolution of O_3 at night. While this result is expected, the agreement supports the hypothesis that no additional reactions of O_3, other than those already present in the model, are necessary to explain the nighttime evolution of O_3 under the stated conditions.

[54] However, not only were the predicted NO_2 mixing ratios for all four plume segments lower than the observed values, but the extent of underprediction systematically grew with increasing processing time (see Figure 17). Furthermore, for a given processing time, the underprediction worsened with increasing $\gamma(N_2O_5)$ values. The latter was due to greater amounts of NO_x converted to HNO_3 at higher values of $\gamma(N_2O_5)$, which suggests that $\gamma(N_2O_5)$ was most likely ~0.001 or less so as to produce the least error in the predicted NO_2 mixing ratios. The systematic underprediction of NO_2 with increasing processing time appears to be because of overestimation of NO_2 due to partial decomposition of N_2O_5 and NO_3 inside the chemiluminescence instrument. As N_2O_5 and NO_3 mixing ratios grew with processing time, so did the overestimation of NO_2. The details of this NO_2 measurement artifact are given in Appendix A.

[55] Because NO_3 and N_2O_5 were not explicitly measured, it was not possible to fully correct the observed (i.e., reported) NO_2 mixing ratios for the measurement artifact. Instead, we applied the measurement artifact to the predicted NO_2 by subjecting the predicted NO, NO_2, N_2O_5, NO_3, PAN, and O_3 mixing ratios at each plume segment to a

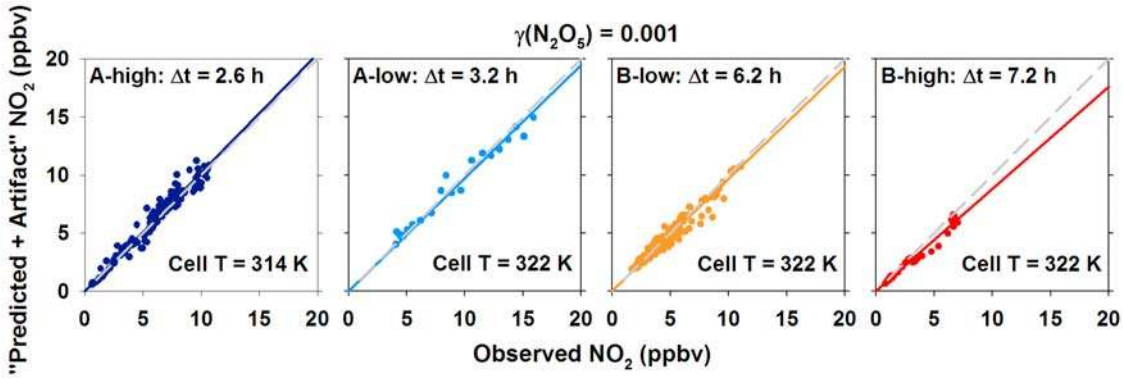

Figure 18. "Predicted + artifact" NO_2 versus observed NO_2 mixing ratios for $\gamma(N_2O_5) = 0.001$. Estimated temperatures in the chemiluminescence photolysis cell were 314 K for the A-high plume segment and 322 K for the remaining three plume segments (see Appendix A for details). Note that after the measurement artifact is aplied to the predicted NO_2 mixing ratios, they are in excellent agreement with the observed values which also contain the measurement artifact.

"model chemiluminescence photolysis cell" and divided the resulting NO mixing ratios by the calibrated conversion efficiency (0.35) to obtain the "predicted + artifact" NO_2 mixing ratios. These NO_2 mixing ratios could then be compared to the observed (reported) values in a consistent manner. As shown in Figure 18, the "predicted + artifact" NO_2 mixing ratios with a negligibly small $\gamma(N_2O_5)$ value of 0.001 were in excellent agreement with the observed NO_2 for all four plume segments. The magnitude of the NO_2 artifact depends on the mixing ratios of NO, NO_2, N_2O_5, NO_3, and PAN going into the cell and the temperature of the cell. For $\gamma(N_2O_5) = 0.001$, the estimated NO_2 artifact ranged between 0.1 and 2.8 ppbv. These values respectively correspond to 12–74% of the NO_2 mixing ratios going into the cell. On the other hand, as shown in the plots in Figure 19 (top), the "predicted + artifact" NO_2 mixing ratios with

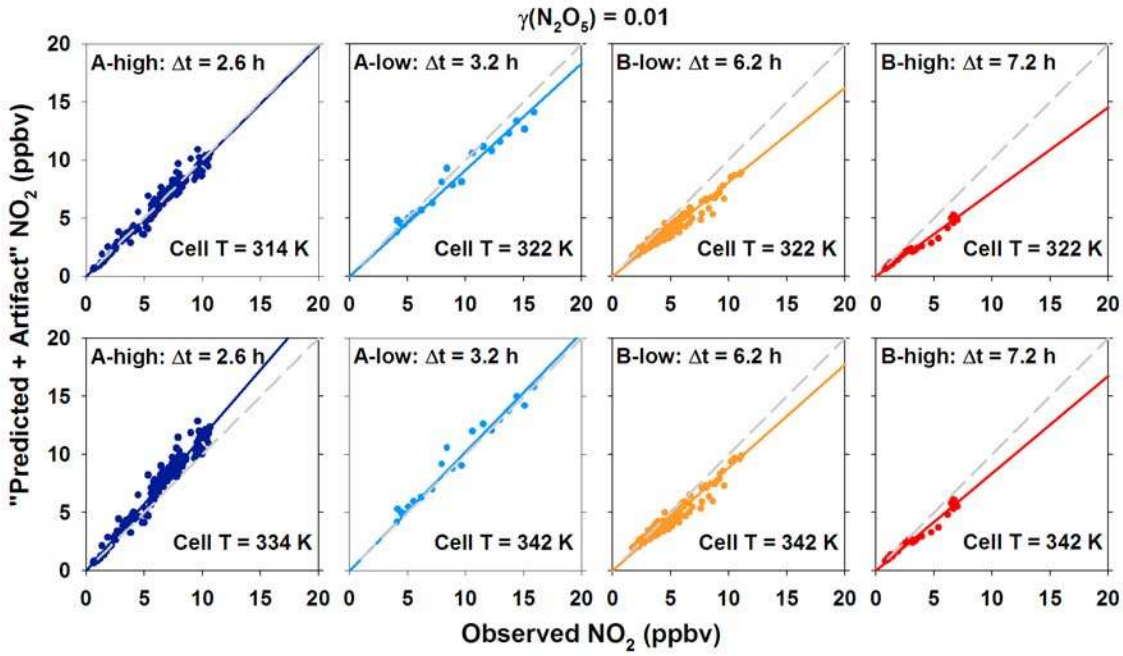

Figure 19. "Predicted + artifact" NO_2 versus observed NO_2 mixing ratios for $\gamma(N_2O_5) = 0.01$. (top) The cell temperatures used are the same as the ones shown in Figure 18. Note that the systematic underprediction still persists after applying the measurement artifact. (bottom) The cell temperatures are assumed to be 20 K higher (i.e., unreasonably high) than those used in the top row. Predicted + artifact NO_2 is higher than that observed in the A-high plume segment while still slightly lower than that observed in the B-low and B-high plume segments.

$\gamma(N_2O_5)$ = 0.01 were still systematically lower than the observed NO_2 values at the four plume segments. Moreover, these discrepancies could not be rectified even when unreasonably high temperatures (i.e., 20 K higher than the estimated values) are assumed in the chemiluminescence cell, as shown in the plots in Figure 19 (bottom).

[56] Based on the above constrained plume modeling analysis, we conclude that the true value of $\gamma(N_2O_5)$ was negligibly small (<0.001) in the Salem Harbor power plant plume under the conditions of this study. This result is consistent with that of *Brown et al.* [2007], who also estimated a negligibly small value for $\gamma(N_2O_5)$ in the Salem Harbor power plant plume during the summertime NEAQS 2004 campaign (i.e., 2 years after this field campaign). A negligibly small $\gamma(N_2O_5)$ value implies that essentially all of the NO_x emitted at night, except for the <0.2 ppbv that was converted to organic nitrates in the present case, would become available for photochemical O_3 formation the following day.

5. Summary, Conclusions, and Future Work

[57] A set of unique observations describing the evolution of aerosol and trace gas chemistry in a nocturnal power plant plume were made during the NAOPEX, which was carried out as part of the summer 2002 NEAQS field campaign in the New England area. A constant-volume, superpressure tetroon, equipped with GPS, radiosonde, and ozonesonde, was successfully used as a Lagrangian tracer to "tag" the Salem Harbor power plant plume soon after sunset on 30 July 2002. Guided by the location of the tetroon in real time, two back-to-back flights were made with the instrumented DOE G-1 aircraft to sample in the plume at increasing downwind distances. Four relatively concentrated plume segments at two distinct altitudes were identified based on the observed SO_2 versus NO_y correlations. The processing time (since emission) for each plume segment was estimated from the relative spatial proximity between the tetroon and the plume segment and the observed vertical wind velocity profiles near the tetroon.

[58] Analysis of the O_3, NO_x, and NO_z measurements in the four plume segments revealed that the total odd oxygen budget was conserved in the plume relative to the nearby background values. The biogenic isoprene mixing ratio in the background air was about 0.3 ppbv while it was completely depleted in the plume. Concentrations of particulate organics, sulfate, and nitrate aerosol were about 1, 1.5, and 0.2 μg m^{-3} higher at the plume peak, respectively, relative to their respective background values of about 4, 1.5, and 0.2 μg m^{-3}. X-ray microanalysis of individual particles sampled within the plume and in background air indicated that these species were internally mixed. At the same time, no evidence was found for any fly ash–type materials within the plume. The in-plume particles were found to be highly acidic, as inferred from the bulk NH_4/SO_4 molar ratios of less than 2. The predicted equilibrium HNO_3 mixing ratios over these particles were unreasonably large, which suggested that the observed particulate nitrate was likely in the form of organic nitrate as opposed to inorganic nitrate ion form. The enhanced particulate organic and nitrate masses observed in the plume were therefore inferred as secondary organic aerosol, possibly formed from the NO_3 radical-initiated oxidation of isoprene, other biogenic VOCs, and their photo-oxidation products that would have been left over in the nocturnal residual layer from the preceding afternoon. The resulting SOA would be composed of organic nitrates [*Barnes et al.*, 1990; *Shepson et al.*, 1996; *Starn et al.*, 1998; *Ng et al.*, 2008].

[59] The enhanced particulate sulfate concentrations observed in the plume were likely due to direct emissions of SO_3/H_2SO_4 from the power plant. A fourfold enhancement in the nucleation-mode (5–20 nm) particle number concentration detected in the nocturnal plume indicated that some of the emitted H_2SO_4 vapors had nucleated to form new particles while the rest had condensed upon preexisting particles. NEXAFS and STXM analyses of particle samples suggested that some sulfate may have been present as organosulfates. While the exact formation mechanisms are still being investigated, laboratory evidence exists for the formation of organosulfates [*Liggio and Li*, 2006; *Liggio et al.*, 2007; *Paulot et al.*, 2009] and nitroxy organosulfates [*Surratt et al.*, 2008] from the reaction of acidic sulfate particles with isoprene, other biogenic VOCs (monoterpenes), as well as their photo-oxidation products such as pinonaldehyde and dihydroxyepoxides, under conditions similar to those found in the nocturnal power plant plume investigated in this study.

[60] NEXAFS analysis of the particle samples also revealed the presence of sp^2 hybridized C = C bonds. The calculated percent of sp^2 hybridization was found to decrease from about 8% in the background air samples to <2% after 6.2 h of processing in the plume. One possible explanation for the observed loss of C = C bonds with processing time is the heterogeneous reaction with elevated levels of NO_3 radicals present in the power plant plume. Such reactions could also form small amounts of organic nitrates in the particulate phase.

[61] A CPM analysis of the aircraft and tetroon observations was performed using the comprehensive trace gas-aerosol chemistry box model MOSAIC. The model successfully reproduced the observed gradual decay of O_3 in the plume, which was attributed to the $O_3 + NO_2$ reaction. The model was also able to successfully reproduce the observed NO_2 mixing ratios after taking into account a measurement artifact due to partial decomposition of NO_2 reservoirs (N_2O_5 and NO_3) in the chemiluminescence instrument. The predicted NO_2 mixing ratios were found to be sensitive to the N_2O_5 heterogeneous hydrolysis uptake coefficient $\gamma((N_2O_5)$. A series of model sensitivity tests then suggested that $\gamma(N_2O_5)$ was likely negligibly small (<0.001) for the aerosol observed in the plume at ambient relative humidities between 60% and 70%. As a result, essentially all of the NO_x emitted at night, except for the <0.2 ppbv that was converted to organic nitrate aerosol in the present case, would become available for photochemical O_3 formation the following day.

[62] These results have significant implications for several scientific and regulatory issues related to the impacts of power plant emissions (and their interactions with biogenic emissions) on air quality and climate. A combination of additional laboratory, field, and modeling studies are needed to (1) investigate the efficacy of NO_3 radical-initiated biogenic SOA formation in nocturnal power plant plumes and the impact of such particles on regional air quality and

radiative forcing; (2) investigate the effect of nighttime SOA formation on the heterogeneous hydrolysis of N_2O_5, and thereby its feedback on photochemical O_3 formation; and (3) understand the origin of the somewhat ubiquitous sp^2 hybridized C = C double bonds observed in organic aerosols and their role in nighttime heterogeneous chemistry.

Appendix A: NO_2 Measurement Artifact

A1. Description of the Chemiluminescence Cell

[63] In the NO_2 measurement system, NO_2 is first converted to NO by photolytic reduction followed by detection as NO based on the chemiluminescence resulting from the reaction with added O_3 [*Springston et al.*, 2005]. The UV source in the photolysis cell was a high-pressure xenon arc lamp through a cold mirror, which reflected light with wavelengths from 350 to 550 nm. The gas residence time inside the NO_2 photolysis cell was 3.5 ± 0.1 s and the NO_2-to-NO conversion efficiency was 34.8%, which was calibrated in the absence of significant amounts of N_2O_5 and NO_3. However, N_2O_5 and NO_3 species were likely present at appreciable levels in the nocturnal power plant plume segments. The thermal decomposition of N_2O_5 to NO_2 + NO_3, photolysis of NO_3 to NO, and other related reactions that would occur inside the photolysis cell would increase the NO mixing ratio exiting the cell, thus artificially increasing the reported NO_2.

A2. Estimation of the Photolysis Rates and Temperatures Inside the Cell

[64] Based on the cell residence time of 3.5 s and NO_2-to-NO conversion efficiency of 35%, the photolysis rate constant for NO_2 was estimated to be 0.125 s^{-1}. Then based on the spectrum of the UV light in the cell, the photolysis rate constant for NO_3 for the NO_2 + $O(^3P)$ channel was estimated as 2.5 s^{-1} using the National Center for Atmospheric Resarch (NCAR) Tropospheric Ultraviolet and Visible model [*Madronich and Flocke*, 1999].

[65] Unfortunately, the temperature inside the photolysis cell was not measured. However, the observed cabin temperature near the cell was ~309 K during the A-high segment and ~312 K during the A-low, B-low, and B-high segments. These temperatures serve as a lower limit for the temperatures inside the cell for the respective plume segments. Also, the ambient air temperature and pressure for the high-altitude plume segments were 293 K and 913 mbar, respectively. The corresponding values for the low-altitude segments were 298 K and 973 mbar. The airstream entering the photolysis cell experienced a drop in pressure down to 400 mbar. The actual cell temperature at any given time would then depend on the temperature of the ambient air coming into the cell, cooling due to adiabatic expansion in the cell, heating caused by the photolysis lamp, and cooling due to heat loss through the cell wall via conduction and convection. While it is difficult to calculate the exact cell temperature, we estimate the upper limit to be about 342 K, which only takes into account heating due to the lamp and cooling due to the adiabatic expansion, whereas cooling due to heat loss via conduction and convection was completely ignored. The heat loss term, which would also depend on the cabin temperature, is expected to be quite significant due to active cooling by a fan on the cell enclosure that pulled hot air out and allowed cool air to come in at the two grates on either end of the cell. As a result, the actual cell temperatures are expected to be only a few degrees (~5 K) warmer than the cabin temperature at any given instance. Taking into account both ambient and cabin temperatures mentioned above, we expect the cell temperatures for the last three plume segments to be up to 8 K warmer than for the first plume segment. Thus, the estimated cell temperatures are 314 K for the first plume segment (A-high) and 322 K for the remaining ones (A-low, B-low, and B-high).

[66] **Acknowledgments.** We thank the chief pilot Bob Hannigan and the PNNL flight crew for once again translating our scientific needs into safe flight operations with the G-1. We gratefully thank the following for their contributions and cooperation in this research effort: Rich Barchet (PNNL) and Katie Shaver (PNNL, summer intern); Alex Pszenny (University of New Hampshire); Chester Suchecki; Rich Coulter (Argonne National Laboratory); Paul Tracy and Lt. Col. John Roadcap (Air Force Research Laboratory, Hanscom AFB); Tim Lachenmeier and Bob Moody (GSSL, Inc.); Walter Komhyr and Jim Wendell (EN-SCI Corp.); Ted Maney (Marine Science Center, Northeastern University); Boston Air Traffic Control and Logan Watch Supervisor; and the town of Nahant, Massachusetts. We also thank Steven Brown (NOAA), Frank Flocke (NCAR), and Timothy Bertram (UW, Seattle) for their insights into the N_2O_5/NO_3 chemistry and many helpful discussions. Support for this research was provided by the Atmospheric Science Program within the Office of Biological and Environmental Research of the DOE. Work by Brookhaven National Laboratory scientists was performed under contracts DE-AC02-98CH10886 and DE-AC06-76RLO 1830. STXM/NEXAFS analysis of particle samples at the Advanced Light Source (ALS) were partially supported by the Director, Office of Science, Office of Basic Energy Sciences, Division of Chemical Sciences, Geosciences, and Biosciences of the U.S. Department of Energy at Lawrence Berkeley National Laboratory under contract DE-AC02-05CH11231. The SEM particle analysis was performed in the Environmental Molecular Sciences Laboratory, a national scientific user facility sponsored by the Department of Energy's Office of Biological and Environmental Research at Pacific Northwest National Laboratory (PNNL). PNNL is operated for the U.S. Department of Energy by Battelle Memorial Institute under contract DE-AC06-76RLO 1830.

References

Angell, J. K. (1961), Use of constant level balloons in meteorology, *Adv. Geophys.*, *8*, 137–219.

Angell, J. K., C. R. Dickson, and W. H. Hoecker Jr. (1976), Tetroon trajectories in the Los Angeles basin defining the source of air reaching the San Bernadino-Riverside area in late afternoon, *J. Appl. Meteorol.*, *15*(3), 197–204, doi:10.1175/1520-0450(1976)015<0197:TTITLA>2.0.CO;2.

Badger, C. L., P. T. Griffiths, I. George, J. P. D. Abbatt, and R. A. Cox (2006), Reactive uptake of N_2O_5 by aerosol particles containing mixtures of humic acid and ammonium sulfate, *J. Phys. Chem. A*, *110*, 6986–6994, doi:10.1021/jp0562678.

Barnes, I., V. Bastian, K. H. Becker, and Z. Tong (1990), Kinetics and products of the reactions of NO_3 with monoalkenes, dialkenes, and monoterpenes, *J. Phys. Chem.*, *94*, 2413–2419, doi:10.1021/j100369a041.

Berkowitz, C. M., J. D. Fast, S. R. Springston, R. J. Larsen, C. W. Spicer, P. V. Doskey, J. M. Hubbe, and R. Plastridge (1998), Formation mechanisms and chemical characteristics of elevated photochemical layers over the northeast United States, *J. Geophys. Res.*, *103*(D9), 10,631–10,647, doi:10.1029/97JD03751.

Bertram, T. H., and J. A. Thornton (2009), Toward a general parameterization of N_2O_5 reactivity on aqueous particles: The competing effects of particle liquid water, nitrate and chloride, *Atmos. Chem. Phys. Discuss.*, *9*, 15,181–15,214.

Brock, C. A., et al. (2002), Particle growth in the plumes of coal-fired power plants, *J. Geophys. Res.*, *107*(D12), 4155, doi:10.1029/2001JD001062.

Brown, S. S., et al. (2009), Reactive uptake coefficients for N205 determined from aircraft measurements during the Second Texas Air Quality Study: Comparison to current model parameterizations, *J. Geophys. Res.*, *114*, D00F10, doi:10.1029/2008JD011679.

Brown, S. S., H. Stark, T. B. Ryerson, E. J. Williams, D. K. Nicks Jr., M. Trainer, F. C. Fehsenfeld, and A. R. Ravishankara (2003), Nitrogen oxides in the nocturnal boundary layer: Simultaneous in situ measurements of NO_3, N_2O_5, NO_2, NO, and O_3, *J. Geophys. Res.*, *108*(D9), 4299, doi:10.1029/2002JD002917.

Brown, S. S., et al. (2004), Nighttime removal of NO_x in the summer marine boundary layer, *Geophys. Res. Lett.*, *31*, L07108, doi:10.1029/2004GL019412.

Brown, S. S., et al. (2006a), Nocturnal odd-oxygen budget and its implications for ozone loss in the lower troposphere, *Geophys. Res. Lett.*, *33*, L08801, doi:10.1029/2006GL025900.

Brown, S., et al. (2006b), Variability in nocturnal nitrogen oxide processing and its role in regional air quality, *Science*, *311*, 67–70, doi:10.1126/science.1120120.

Brown, S., et al. (2007), Vertical profiles in NO_3 and N_2O_5 measured from an aircraft: Results from the NOAA P-3 and surface platforms during the New England Air Quality Study 2004, *J. Geophys. Res.*, *112*, D22304, doi:10.1029/2007JD008883.

Businger, S., S. R. Chiswell, and W. C. Ulmer (1996), Balloons as a Lagrangian measurement platform for atmospheric research, *J. Geophys. Res.*, *101*(D2), 4363–4376, doi:10.1029/95JD00559.

Businger, S., R. Johnson, J. Katzfey, S. Siems, and Q. Wang (1999), Smart tetroons for Lagrangian air-mass tracking, *J. Geophys. Res.*, *104*(D9), 11,709–11,722, doi:10.1029/1998JD100094.

Buzorius, G., C. S. McNaughton, A. D. Clarke, D. S. Covert, B. Blomquist, K. Nielsen, and F. J. Brechtel (2004), Secondary aerosol formation in continental outflow conditions during ACE-Asia, *J. Geophys. Res.*, *109*, D24203, doi:10.1029/2004JD004749.

Cichanowicz, J. E. (2007), Estimating total sulfuric acid emissions from stationary power plants, *Rep. 1014773*, Electr. Power Res. Inst., Palo Alto, Calif.

Damle, A. S., D. S. Ensor, and M. B. Ranade (1982), Coal combustion aerosol formation mechanisms: A review, *Aerosol Sci. Technol.*, *1*(1), 119–133, doi:10.1080/02786828208958582.

Dentener, F. J., and P. J. Crutzen (1993), Reaction of N_2O_5 on tropospheric aerosols: Impact on the global distributions of NO_x, O_3, and OH, *J. Geophys. Res.*, *98*(D4), 7149–7163, doi:10.1029/92JD02979.

Docherty, K. S., and P. J. Ziemann (2006), Reaction of oleic acid particles with NO_3 radicals: Products, mechanism, and implications for radical-initiated organic aerosol oxidation, *J. Phys. Chem. A*, *110*, 3567–3577, doi:10.1021/jp0582383.

Draxler, R. R., and G. D. Rolph (2003), HYSPLIT (HYbrid Single-Particle Lagrangian Integrated Trajectory) Model access via NOAA ARL READY Website (http://www.arl.noaa.gov/ready/hysplit4.html). NOAA Air Resources Laboratory, Silver Spring, MD.

Fehsenfeld, F. C., et al. (2006), International Consortium for Atmospheric Research on Transport and Transformation (ICARTT): North America to Europe–Overview of the 2004 summer field study, *J. Geophys. Res.*, *111*, D23S01, doi:10.1029/2006JD007829.

Folkers, M., T. F. Mentel, and A. Wahner (2003), Influence of an organic coating on the reactivity of aqueous aerosols probed by the heterogeneous hydrolysis of N_2O_5, *Geophys. Res. Lett.*, *30*(12), 1644, doi:10.1029/2003GL017168.

Forster, P. V., et al. (2007), Changes in atmospheric constituents and in radiative forcing, in *Climate Change 2007: The Physical Science Basis. Contribution of Working Group I to the Fourth Assessment Report of the Intergovernmental Panel on Climate Change*, edited by S. Solomon et al., pp. 129–234, Cambridge Univ. Press, Cambridge, U. K.

Frost, G. J., et al. (2006), Effects of changing power plant NO_x emissions on ozone in the eastern United States: Proof of concept, *J. Geophys. Res.*, *111*, D12306, doi:10.1029/2005JD006354.

Fry, J. L., et al. (2009), Organic nitrate and secondary organic aerosol yield from NO_3 oxidation of β-pinene evaluated using a gas-phase kinetics/aerosol partitioning model, *Atmos. Chem. Phys.*, *9*, 1431–1449.

Gillani, N. V., J. F. Meagher, R. J. Valente, R. E. Imhoff, R. L. Tanner, and M. Luria (1998), Relative production of ozone and nitrates in urban and rural power plant plumes 1. Composite results based on data from 10 field measurement days, *J. Geophys. Res.*, *103*(D17), 22,593–22,615, doi:10.1029/98JD00966.

Goldstein, H. L., and C. W. Siegmund (1976), Influence of heavy fuel oil composition and boiler combustion conditions on particulate emissions, *Environ. Sci. Technol.*, *10*, 1109–1114, doi:10.1021/es60122a006.

Gross, S., and A. K. Bertram (2009), Products and kinetics of the reactions of an alkane monolayer and a terminal alkene monolayer with NO_3 radicals, *J. Geophys. Res.*, *114*, D02307, doi:10.1029/2008JD010987.

Hallquist, M., D. J. Stewart, S. K. Stephenson, and R. A. Cox (2003), Hydrolysis of N_2O_5 on sub-micron sulfate aerosols, *Phys. Chem. Chem. Phys.*, *5*, 3453–3463, doi:10.1039/b301827j.

Hegg, D. A., P. V. Hobbs, and J. H. Lyons (1985), Field studies of a power plant plume in the arid southwestern United States, *Atmos. Environ.*, *19*, 1147–1167, doi:10.1016/0004-6981(85)90199-4.

Hobbs, P. V., and D. A. Hegg (1982), Sulfate and nitrate mass distributions in the near fields of some coal-fired power plants, *Atmos. Environ.*, *16*, 2657–2662, doi:10.1016/0004-6981(82)90347-X.

Hoecker, W. H., Jr. (1975), A universal procedure for deploying constant-volume balloons and for deriving vertical air speeds from them, *J. Appl. Meteorol.*, *14*, 1118–1124, doi:10.1175/1520-0450(1975)014<1118:AUPFDC>2.0.CO;2.

Hopkins, R. J., et al. (2007a), Correlations between optical, chemical, and physical properties of biomass burn aerosols, *Geophys. Res. Lett.*, *34*, L18806, doi:10.1029/2007GL030502.

Hopkins, R. J., et al. (2007b), Chemical bonding and structure of black carbon reference materials and individual carbonaceous atmospheric aerosols, *J. Aerosol Sci.*, *38*(6), 573–591, doi:10.1016/j.jaerosci.2007.03.009.

Hopkins, R. J., et al. (2008), Chemical speciation of sulfur in marine cloud droplets and particles: Analysis of individual particles from the marine boundary layer over the California current, *J. Geophys. Res.*, *113*(D4), D04209, doi:10.1029/2007JD008954.

Hu, J. H., and J. P. D. Abbatt (1997), Reaction probability for N_2O_5 hydrolysis on sulfuric acid and ammonium sulfate aerosols at room temperature, *J. Phys. Chem. A*, *101*, 871–878, doi:10.1021/jp9627436.

Huebert, B. J., A. Pszenny, and B. Blomquist (1996), The ASTEX/MAGE experiment, *J. Geophys. Res.*, *101*(D2), 4319–4329, doi:10.1029/95JD01531.

Hung, H. M., Y. Katrib, and S. T. Martin (2005), Products and mechanisms of the reaction of oleic acid with ozone and nitrate radical, *J. Phys. Chem. A*, *109*, 4517–4530, doi:10.1021/jp0500900.

Jacob, D. J. (2000), Heterogeneous chemistry and tropospheric ozone, *Atmos. Environ.*, *34*, 2131–2159, doi:10.1016/S1352-2310(99)00462-8.

Jacob, D. J., et al. (1996), Origin of ozone and NO_x in the tropical troposphere: A photochemical analysis of aircraft observations over the South Atlantic basin, *J. Geophys. Res.*, *101*(D19), 24,235–24,250, doi:10.1029/96JD00336.

Jayne, J. T., D. C. Leard, X. Zhang, P. Davidovits, K. A. Smith, C. E. Kolb, and D. R. Worsnop (2000), Development of an aerosol mass spectrometer for size and composition analysis of submicron particles, *Aerosol Sci. Technol.*, *33*, 49–70, doi:10.1080/027868200410840.

Johnson, D. W., et al. (2000a), An overview of the Lagrangian experiments undertaken during the North Atlantic regional Aerosol Characterisation Experiment (ACE-2), *Tellus*, *52B*, 290–320.

Johnson, R., S. Businger, and A. Baerman (2000b), Lagrangian air mass tracking with smart balloons during ACE-2, *Tellus*, *52B*, 321–334.

Kane, S. M., F. Caloz, and M.-T. Leu (2001), Heterogeneous uptake of gaseous N_2O_5 by $(NH_4)_2SO_4$, NH_4HSO_4, and H_2SO_4 aerosols, *J. Phys. Chem. A*, *105*, 6465–6470, doi:10.1021/jp010490x.

Kleinman, L. I., et al. (2007), Aircraft observations of aerosol composition and ageing in New England and Mid-Atlantic States during the summer 2002 New England Air Quality Study field campaign, *J. Geophys. Res.*, *112*, D09310, doi:10.1029/2006JD007786.

Komhyr, W. D. (1969), Electrochemical concentration cells for gas analysis, *Ann. Geophys.*, *25*, 203–210.

Komhyr, W. D., R. A. Barnes, G. B. Brothers, J. A. Lathrop, and D. P. Opperman (1995), Electrochemical concentration cell ozonesonde performance evaluation during STOIC 1989, *J. Geophys. Res.*, *100*(D5), 9231–9244, doi:10.1029/94JD02175.

Kroll, J. H., N. L. Ng, S. M. Murphy, R. C. Flagan, and J. H. Seinfeld (2005), Secondary organic aerosol formation from isoprene photooxidation under high-NO_x conditions, *Geophys. Res. Lett.*, *32*, L18808, doi:10.1029/2005GL023637.

Kroll, J. H., N. L. Ng, S. M. Murphy, R. C. Flagan, and J. H. Seinfeld (2006), Secondary organic aerosol formation from isoprene photooxidation, *Environ. Sci. Technol.*, *40*, 1869–1877, doi:10.1021/es0524301.

Laskin, A., M. J. Iedema, and J. P. Cowin (2003), Time-resolved aerosol collector for CCSEM/EDX single-particle analysis, *Aerosol Sci. Technol.*, *37*, 246–260, doi:10.1080/02786820300945.

Laskin, A., J. P. Cowin, and M. J. Iedema (2006), Analysis of individual environmental particles using modern methods of electron microscopy and X-ray microanalysis, *J. Electron Spectrosc. Relat. Phenom.*, *150*, 260–274, doi:10.1016/j.elspec.2005.06.008.

Liggio, J., and S.-M. Li (2006), Organosulfate formation during the uptake of pinonaldehyde on acidic sulfate aerosols, *Geophys. Res. Lett.*, *33*, L13808, doi:10.1029/2006GL026079.

Liggio, J., S.-M. Li, J. R. Brook, and C. Mihele (2007), Direct polymerization of isoprene and α-pinene on acidic aerosols, *Geophys. Res. Lett.*, *34*, L05814, doi:10.1029/2006GL028468.

Madronich, S., and S. Flocke (1999), The role of solar radiation in atmospheric chemistry, in *Handbook of Environmental Chemistry*, edited by P. Boule, pp. 1–26, Springer, Heidelberg, Germany.

Malm, W. C., J. F. Sisler, D. Huffman, R. A. Eldred, and T. A. Cahill (1994), Spatial and seasonal trends in particle concentration and optical extinction in the United States, *J. Geophys. Res.*, *99*(D1), 1347–1370, doi:10.1029/93JD02916.

Mao, H., R. Talbot, D. Troop, R. Johnson, S. Businger, and A. M. Thompson (2006), Smart balloon observations over the North Atlantic: O_3 data analysis and modeling, *J. Geophys. Res.*, *111*, D23S56, doi:10.1029/2005JD006507.

Maria, S. F., et al. (2004), Organic aerosol growth mechanisms and their climate-forcing implications, *Science*, *306*(5703), 1921–1924, doi:10.1126/science.1103491.

McMurry, P. H., D. J. Rader, and J. L. Stith (1981), Studies of aerosol formation in power plant plumes—I. Growth laws for secondary aerosols in power plant plumes: Implications for chemical conversion mechanisms, *Atmos. Environ.*, *15*, 2315–2327, doi:10.1016/0004-6981(81)90262-6.

McNeill, V. F., J. Patterson, G. M. Wolfe, and J. A. Thornton (2006), The effect of varying levels of surfactant on the reactive uptake of N_2O_5 to aqueous aerosol, *Atmos. Chem. Phys.*, *6*, 1635–1644.

Meagher, J. F., L. Stockburger, E. M. Bailey, and O. Huff (1978), The oxidation of sulfur dioxide to sulfate aerosols in the plume of a coal-fired power plant, *Atmos. Environ.*, *12*, 2197–2203, doi:10.1016/0004-6981(78)90175-0.

Mentel, T. F., M. Sohn, and A. Wahner (1999), Nitrate effect in the heterogeneous hydrolysis of dinitrogen pentoxide on aqueous aerosols, *Phys. Chem. Chem. Phys.*, *1*, 5451–5457, doi:10.1039/a905338g.

Michelsen, H. A., et al. (2007), Particle formation from pulsed laser irradiation of soot aggregates studied with a scanning mobility particle sizer, a transmission electron microscope, and a scanning transmission X-ray microscope, *Appl. Opt.*, *46*(6), 959–977, doi:10.1364/AO.46.000959.

Moffet, R. C., et al. (2008), Characterization of aerosols containing Zn, Pb, and Cl from an industrial region of Mexico City, *Environ. Sci. Technol.*, *42*(19), 7091–7097, doi:10.1021/es7030483.

Moffet, R. C., et al. (2009), Microscopic characterization of carbonaceous aerosol particle aging in the outflow from Mexico City, *Atmos. Chem. Phys. Discuss.*, *9*, 16,993–17,033.

Moise, T., R. K. Talukdar, G. J. Frost, R. W. Fox, and Y. Rudich (2002), Reactive uptake of NO_3 by liquid and frozen organics, *J. Geophys. Res.*, *107*(D2), 4014, doi:10.1029/2001JD000334.

Mozurkewich, M., and J. G. Calvert (1988), Reaction probability of N_2O_5 on aqueous aerosols, *J. Geophys. Res.*, *93*(D12), 15,889–15,896, doi:10.1029/JD093iD12p15889.

Msibi, I. M., Y. Li, J. P. Shi, and R. M. Harrison (1994), Determination of heterogeneous reaction probability using deposition profile measurement in an annular reactor: Application to the N_2O_5/H_2O reaction, *J. Atmos. Chem.*, *18*, 291–300, doi:10.1007/BF00696784.

Mueller, S. F., and R. E. Imhoff (1994), Estimates of particle formation and growth in coal-fired boiler exhaust—I. Observations, *Atmos. Environ.*, *28*, 595–602, doi:10.1016/1352-2310(94)90035-3.

Ng, N. L., et al. (2007), Effect of NO_x level on secondary organic aerosol (SOA) formation from the photooxidation of terpenes, *Atmos. Chem. Phys.*, *7*, 5159–5174.

Ng, N. L., et al. (2008), Secondary organic aerosol (SOA) formation from reaction of isoprene with nitrate radicals (NO_3), *Atmos. Chem. Phys.*, *8*, 4117–4140.

Norris, W. B., S. F. Mueller, and J. E. Langstaff (1999), Estimates of sulfate deposition in the middle eastern United States: 1975, 1990, and 2010, *J. Air Waste Manage. Assoc.*, *49*(6), 655–668.

Nozière, B., P. Dziedzic, and A. Córdova (2007), Formation of secondary light-absorbing "fulvic-like" oligomers: A common process in aqueous and ionic atmospheric particles? *Geophys. Res. Lett.*, *34*, L21812, doi:10.1029/2007GL031300.

Nozière, B., P. Dziedzic, and A. Córdova (2009), Common inorganic ions are efficient catalysts for organic reactions in atmospheric aerosols and other natural environments, *Atmos. Chem. Phys. Discuss.*, *9*, 1–21.

Paulot, F., J. D. Crounse, H. G. Kjaergaard, A. Kürten, J. M. St. Clair, J. H. Seinfeld, and P. O. Wennberg (2009), Unexpected epoxide formation in the gas-phase photooxidation of isoprene, *Science*, *325*, 730–733, doi:10.1126/science.1172910.

Querol, X., A. Alastuey, A. Lopez-Soler, E. Mantilla, and F. Plana (1996), Mineral composition of atmospheric particulates around a large coal-fired power station, *Atmos. Environ.*, *30*, 3557–3572, doi:10.1016/1352-2310(96)00108-2.

Real, E., et al. (2008), Lagrangian analysis of low altitude anthropogenic plume processing across the North Atlantic, *Atmos. Chem. Phys.*, *8*, 7737–7754.

Riddle, E. E., P. B. Voss, A. Stohl, D. Holcomb, D. Maczka, K. Washburn, and R. W. Talbot (2006), Trajectory model validation using newly developed altitude-controlled balloons during the International Consortium for Atmospheric Research on Transport and Transformations 2004 campaign, *J. Geophys. Res.*, *111*, D23S57, doi:10.1029/2006JD007456.

Rogge, W. F., L. M. Hildemann, M. A. Mazurek, G. R. Cass, and B. R. T. Simoneit (1997), Sources of fine organic aerosol. 8. Boilers burning no. 2 distillate fuel oil, *Environ. Sci. Technol.*, *31*, 2731–2737, doi:10.1021/es9609563.

Rollins, A. W., et al. (2009), Isoprene oxidation by nitrate radical: Alkyl nitrate and secondary organic aerosol yields, *Atmos. Chem. Phys.*, *9*, 6685–6703.

Ryerson, T. B., et al. (2001), Observations of ozone formation in power plant plumes and implications for ozone control strategies, *Science*, *292*, 719–723, doi:10.1126/science.1058113.

Shepson, P. B., E. Mackay, and K. Muthuramu (1996), Henry's law constants and removal processes for several atmospheric beta-hydroxy alkyl nitrates, *Environ. Sci. Technol.*, *30*, 3618–3623, doi:10.1021/es960538y.

Smith, T. B., D. L. Blumenthal, J. A. Anderson, and A. H. Vanderpol (1978), Transport of SO_2 in power plant plumes: Day and night, *Atmos. Environ.*, *12*, 605–611, doi:10.1016/0004-6981(78)90240-8.

Springston, S. R., L. I. Kleinman, F. Brechtel, Y.-N. Lee, L. J. Nunnermacker, and J. Wang (2005), Chemical evolution of an isolated power plant plume during the TexAQS 2000 study, *Atmos. Environ.*, *39*, 3431–3443, doi:10.1016/j.atmosenv.2005.01.060.

Srivastava, R. K., C. A. Miller, C. Erickson, and R. Jambhekar (2004), Emissions of sulfur trioxide from coal-fired power plants, *J. Air Waste Manage. Assoc.*, *54*(6), 750–762.

Stark, H., S. S. Brown, P. D. Goldan, M. Aldener, W. C. Kuster, R. Jakoubek, F. C. Fehsenfeld, J. Meagher, T. S. Bates, and A. R. Ravishankara (2007), Influence of nitrate radical on the oxidation of dimethyl sulfide in a polluted marine environment, *J. Geophys. Res.*, *112*, D10S10, doi:10.1029/2006JD007669.

Starn, T. K., P. B. Shepson, S. B. Bertman, D. D. Riemer, R. G. Zika, and K. Olszyna (1998), Nighttime isoprene chemistry at an urban-impacted forest site, *J. Geophys. Res.*, *103*(D17), 22,437–22,447, doi:10.1029/98JD01201.

Surratt, J. D., et al. (2008), Organosulfate formation in biogenic secondary organic aerosol, *J. Phys. Chem. A*, *112*, 8345–8378, doi:10.1021/jp802310p.

Takahama, S., S. Gilardoni, L. M. Russell, and A. L. D. Kilcoyne (2007), Classification of multiple types of organic carbon composition in atmospheric particles by scanning transmission X-ray microscopy analysis, *Atmos. Environ.*, *41*, 9435–9451, doi:10.1016/j.atmosenv.2007.08.051.

Takahama, S., et al. (2008), Single-particle oxidation state and morphology of atmospheric iron aerosols, *J. Geophys. Res.*, *113*, D22202, doi:10.1029/2008JD009810.

Thornton, J. A., and J. P. D. Abbatt (2005), N_2O_5 reaction on submicron sea salt aerosol: Kinetics, products, and the effect of surface active organics, *J. Phys. Chem.*, *109*, 10,004–10,012.

Thornton, J. A., C. F. Braban, and J. P. D. Abbatt (2003), N_2O_5 hydrolysis on sub-micron organic aerosols: The effect of relative humidity, particle phase, and particle size, *Phys. Chem. Chem. Phys.*, *5*, 4593–4603, doi:10.1039/b307498f.

Tivanski, A. V., et al. (2007), Oxygenated interface on biomass burn tar balls determined by single particle scanning transmission X-ray microscopy, *J. Phys. Chem. A*, *111*(25), 5448–5458, doi:10.1021/jp070155u.

Unger, N., D. T. Shindell, D. M. Koch, and D. G. Streets (2006), Cross influences of ozone and sulfate precursor emissions changes on air quality and climate, *Proc. Natl. Acad. Sci. U. S. A.*, *101*, 16,109–16,114.

Van Doren, J. M., L. R. Watson, P. Davidovits, D. R. Worsnop, M. S. Zahniser, and C. E. Kolb (1990), Temperature dependence of the uptake coefficients of HNO_3, HCl, and N_2O_5 by water droplets, *J. Phys. Chem.*, *94*, 3265–3269, doi:10.1021/j100371a009.

Wahner, A., T. F. Mentel, M. Sohn, and J. Stier (1998), Heterogeneous reaction of N_2O_5 on sodium nitrate aerosol, *J. Geophys. Res.*, *103*(D23), 31,103–31,112, doi:10.1029/1998JD100022.

Wexler, A. S., and S. L. Clegg (2002), Atmospheric aerosol models for systems including the ions H^+, NH_4^+, Na^+, SO_4^{2-}, NO_3^-, Cl^-, Br^-, and H_2O, *J. Geophys. Res.*, *107*(D14), 4207, doi:10.1029/2001JD000451.

Whitby, K. T., B. K. Cantrell, and D. B. Kittelson (1978), Nuclei formation rates in a coal-fired power plant plume, *Atmos. Environ.*, *12*, 313–321, doi:10.1016/0004-6981(78)90213-5.

Wilson, J. C., and P. H. McMurry (1981), Studies of aerosol formation in power plant plumes—II. Secondary aerosol formation in the Navajo generating station plume, *Atmos. Environ.*, *15*, 2329–2339, doi:10.1016/0004-6981(81)90263-8.

Zak, B. D. (1981), Lagrangian measurements of sulfur dioxide to sulfate conversion rates, *Atmos. Environ.*, *15*, 2583–2591, doi:10.1016/0004-6981(81)90075-5.

Zaveri, R. A., and L. K. Peters (1999), A new lumped structure photochemical mechanism for large-scale applications, *J. Geophys. Res.*, *104*, 30,387–30,415.

Zaveri, R. A., C. M. Berkowitz, L. I. Kleinman, S. R. Springston, P. V. Doskey, W. A. Lonneman, and C. W. Spicer (2003), Ozone production efficiency and NO_x depletion in an urban plume: Interpretation of field

observations and implications for evaluating O_3-NO_x−VOC sensitivity, *J. Geophys. Res.*, *108*(D14), 4436, doi:10.1029/2002JD003144.

Zaveri, R. A., R. C. Easter, and A. S. Wexler (2005a), A new method for multicomponent activity coefficients of electrolytes in aqueous atmospheric aerosols, *J. Geophys. Res.*, *110*, D02201, doi:10.1029/2004JD004681.

Zaveri, R. A., R. C. Easter, and L. K. Peters (2005b), A computationally efficient Multicomponent Equilibrium Solver for Aerosols (MESA), *J. Geophys. Res.*, *110*, D24203, doi:10.1029/2004JD005618.

Zaveri, R. A., R. C. Easter, J. D. Fast, and L. K. Peters (2008), Model for Simulating Aerosol Interactions and Chemistry (MOSAIC), *J. Geophys. Res.*, *113*, D13204, doi:10.1029/2007JD008782.

C. M. Berkowitz, J. M. Hubbe, M. S. Pekour, and R. A. Zaveri, Atmospheric Sciences and Global Change Division, Pacific Northwest National Laboratory, Richland, WA 99352, USA. (rahul.zaveri@pnl.gov)

F. J. Brechtel, Brechtel Manufacturing, Inc., Hayward, CA 94544, USA.

M. K. Gilles, Chemical Sciences Division, Lawrence Berkeley National Laboratory, Berkeley, CA 94720, USA.

J. T. Jayne, T. B. Onasch, and D. R. Worsnop, Aerodyne Research, Inc., Billerica, MA 01821, USA.

L. I. Kleinman and S. R. Springston, Environmental Sciences Department, Brookhaven National Laboratory, Upton, NY 11973, USA.

A. Laskin, Environmental Molecular Sciences Laboratory, Pacific Northwest National Laboratory, Richland, WA 99352, USA.

S. Madronich, National Center for Atmospheric Research, Boulder, CO 80307, USA.

J. A. Thornton, Department of Atmospheric Sciences, University of Washington, Seattle, WA 98195, USA.

A. V. Tivanski, Department of Chemistry, University of Iowa, Iowa City, IA 52242, USA.